00029
Issued November 2000

Aerofoil and wing pitching moment coefficient at zero angle of attack due to deployment of leading-edge high-lift devices

Endorsed by
The Royal Aeronautical Society

ESDU DATA ITEMS

Data Items provide validated information in engineering design and analysis for use by, or under the supervision of, professionally qualified engineers. The data are founded on an evaluation of all the relevant information, both published and unpublished, and are invariably supported by original work of ESDU staff engineers or consultants. The whole process is subject to independent review for which crucial support is provided by industrial companies, government research laboratories, universities and others from around the world through the participation of some of their leading experts on ESDU Technical Committees. This process ensures that the results of much valuable work (theoretical, experimental and operational), which may not be widely available or in a readily usable form, can be communicated concisely and accurately to the engineering community.

We are constantly striving to develop new work and review data already issued. Any comments arising out of your use of our data, or any suggestions for new topics or information that might lead to improvements, will help us to provide a better service.

THE PREPARATION OF THIS DATA ITEM

The work on this particular Data Item was monitored and guided by the Aerodynamics Committee. This Committee first met in 1942 and now has the following membership:

Chairman	
Mr H.C. Garner	— Independent
Members	
Dr M.Z. Bouter*	— Raytheon Aircraft Co., Wichita, Kansas, USA
Mr P.D. Chappell	— Independent
Dr P.C. Dexter	— BAE SYSTEMS, Advanced Technology Centre, Sowerby
Mr J.R.J. Dovey	— Independent
Dr K.P. Garry	— Cranfield University
Mr D.H. Graham*	— Northrop Grumman Corp., El Segundo, CA, USA
Mr M.J. Green	— Independent
Dr H.P. Horton	— Queen Mary and Westfield College, University of London
Mr M. Jager*	— Boeing, Long Beach, CA, USA
Dr E.H. Kitchen	— Rolls-Royce Commercial Aero Engines Ltd, Derby
Miss M. Maina	— Aircraft Research Association Ltd
Mr M. Maurel	— Aérospatiale, Toulouse, France
Mr C.M. Newbold	— Defence Evaluation and Research Agency, Farnborough
Mr J.B. Newton	— BAE SYSTEMS, Military Aircraft and Aerostructures, Warton
Mr M.J. Pow	— BAE SYSTEMS, Airbus, Filton
Mr R. Sanderson	— Daimler-Benz Aerospace Airbus, GmbH, Bremen, Germany
Mr E. Totland	— Saab AB, Linköping, Sweden
Mr J. Tweedie	— Short Brothers plc, Belfast
Mr A.J. Wells	— BAE SYSTEMS, Regional Aircraft, Woodford

* Corresponding Member.

The technical work involved in the assessment of the available information and the development and subsequent construction of the Data Item method was carried out under contract to ESDU by Mr J.R.J. Dovey.

The person with overall responsibility for the work in this subject area is Mr R.W. Gilbey, Head of Aircraft Aerodynamics Group.

AEROFOIL AND WING PITCHING MOMENT COEFFICIENT AT ZERO ANGLE OF ATTACK DUE TO DEPLOYMENT OF LEADING-EDGE HIGH-LIFT DEVICES AT LOW SPEEDS

CONTENTS

		Page
1.	NOTATION AND UNITS	1
2.	INTRODUCTION	5
3.	PREDICTION METHOD	5
3.1	Determination of $\Delta C'_{L0l}$	5
3.1.1	Plain leading-edge flaps and drooped leading edges	7
3.1.2	Slats and vented Krüger flaps	8
3.1.3	Krüger flaps and sealed slats	10
3.2	Aerofoil Pitching Moment Coefficient Increment ΔC_{mla0}	12
3.3	Wing Pitching Moment Coefficient Increment ΔC_{mlwa0}	13
4.	EFFECTS OF MACH NUMBER AND REYNOLDS NUMBER	14
4.1	Mach Number Effects	14
4.2	Reynolds Number Effects	14
5.	APPLICABILITY AND ACCURACY	15
5.1	Applicability	15
5.1.1	Aerofoils	15
5.1.2	Wings	15
5.2	Accuracy	16
5.2.1	Aerofoils	16
5.2.2	Wings	18
6.	DERIVATION AND REFERENCES	19
6.1	Derivation	19
6.1.1	ESDU Data Items	19
6.1.2	Wind-tunnel test reports	19
6.1.3	Theory	21
6.2	References	21
7.	EXAMPLES	22
7.1	Example 1: Pitching Moment Increment due to a Leading-edge Slat on an Aerofoil	22
7.2	Example 2: Pitching Moment Increment due to a Leading-edge Slat on a Wing	26
	FIGURES 1 to 3	28 to 32

AEROFOIL AND WING PITCHING MOMENT COEFFICIENT AT ZERO ANGLE OF ATTACK DUE TO DEPLOYMENT OF LEADING-EDGE HIGH-LIFT DEVICES AT LOW SPEEDS

1. NOTATION AND UNITS

		SI	*British*
A	aspect ratio, $2s/\bar{c}$		
a, b	construction lengths in Sketch 3.2c	m	ft
a_l	theoretical rate of change of lift with leading-edge device deflection, Equation (3.3)	rad^{-1}	rad^{-1}
$(a_1)_0$	basic aerofoil lift-curve slope in incompressible flow	rad^{-1}	rad^{-1}
C_L	lift coefficient; (*lift per unit span*)/qc for aerofoil, (*lift*)/qS for wing		
C_{L0}	C_L at zero angle of attack for aerofoil		
ΔC_{L0l}	increment in lift coefficient at zero angle of attack due to deployment of leading-edge device on aerofoil, based on c (see Item No. 94027, Derivation 2)		
$\Delta C'_{L0l}$	increment in lift coefficient at zero angle of attack due to deployment of leading-edge device on aerofoil, based on c', Equation (3.1), $\Delta C_{L0l}(c/c')$, (see Item No. 94027, Derivation 2)		
$[\Delta C'_{L0l}]_1$	contribution to $\Delta C'_{L0l}$ dependent on leading-edge device type and deflection, Equation (3.2)		
$[\Delta C'_{L0l}]_2$	contribution to $\Delta C'_{L0l}$ dependent on leading-edge device type, see Table 3.1		
C_m	pitching moment coefficient; (*pitching moment per unit span*)/qc^2 for aerofoil, referenced to c/4, (*pitching moment*)/$qS\bar{\bar{c}}$ for wing, referenced to $\bar{\bar{c}}$/4, see Sketch 1.1		
C_{m0}	C_m for aerofoil zero lift, see Section 3.2		
C_{m0i}	inviscid value of C_{m0}		
$C_{m\alpha 0}$	pitching moment coefficient at zero angle of attack for aerofoil, based on c^2 and referenced to c/4, approximated as C_{m0}, see Section 3.2		
$\Delta C_{ml\alpha 0}$	increment in pitching moment coefficient at zero angle of attack due to deployment of leading-edge device on aerofoil, based on c^2 and referenced to c/4, see Equation (3.12)		

Issued November 2000 – 32 pages

$\Delta C'_{ml\alpha 0}$	increment in pitching moment coefficient at zero angle of attack due to deployment of leading-edge device on aerofoil, based on c'^2 and referenced to $c'/4$, see Equation (3.13)		
$\Delta C_{mlw\alpha 0}$	increment in pitching moment coefficient at zero angle of attack due to deployment of leading-edge device on wing, based on $S\bar{\bar{c}}$ and referenced to $\bar{\bar{c}}/4$, see Equation (3.18)		
c	basic (plain) aerofoil chord or wing chord at mid-span of device (*i.e.* chord with high-lift devices undeployed), see Sketch 1.1	m	ft
c'	extended aerofoil chord, *i.e.* chord with leading-edge device deployed, see Sketches 3.1 to 3.3	m	ft
$\bar{c}$	wing geometric mean chord	m	ft
$\bar{\bar{c}}$	wing aerodynamic mean chord (see Item No. 76003, Reference 29)	m	ft
c_{el}	effective chord of leading-edge device, see Table 3.1	m	ft
c_l	chord of leading-edge device, see Sketches 3.1 to 3.3	m	ft
c'_l	extended chord of leading-edge device, see Sketches 3.1 to 3.3	m	ft
Δc_l	chord extension due to deployment of leading-edge device, see Sketches 3.1 to 3.3	m	ft
c_r	wing root (centre-line) chord, see Sketch 1.1	m	ft
F	viscous correction factor used in calculation of C_{m0}, see Equation (3.17)		
H_l	height of trailing-edge of slat or Krüger flap above aerofoil chord-line, see Sketches 3.2 and 3.3	m	ft
h_{2l}	centre of incremental lift at zero angle of attack due to leading-edge device deployment on aerofoil section expressed as fraction of basic aerofoil chord, measured positive aft from aerofoil quarter-chord position		
h'_{2l}	empirical centre of incremental lift at zero angle of attack due to leading-edge device angular deflection on aerofoil section expressed as fraction of extended chord, measured positive aft from extended aerofoil quarter-chord position, see Equation (3.15)		
h'_{2lT}	theoretical value (always negative) on which h'_{2l} is based, see Equation (3.14a) and Figure 1		
K	part-span factor; pitching moment coefficient increment due to part-span leading-edge devices extending symmetrically from wing centre-line divided by pitching moment coefficient increment due to full-span leading-edge devices at same deflection angle, Figure 2		
K_l	leading-edge device type correlation factor, see Table 3.2		

$K_{l\Lambda}$	leading-edge device type correlation factor for wing sweep, see Table 3.2		
K_m	leading-edge device type correlation factor, see Table 3.2		
K_i	value of K corresponding to $\eta = \eta_i$, required in Equation (3.18)		
K_o	value of K corresponding to $\eta = \eta_o$, required in Equation (3.18)		
K_Λ	part-span factor dependent on wing sweep effect, Equation (3.19) and Figures 3a to 3f		
$K_{\Lambda i}$	value of K_Λ corresponding to $\eta = \eta_i$, required in Equation (3.18)		
$K_{\Lambda o}$	value of K_Λ corresponding to $\eta = \eta_o$, required in Equation (3.18)		
K_0	correlation factor in Equation (3.2), dependent on type of leading-edge device, see Table 3.1		
L_l	overlap between trailing edge of deployed slat or vented Krüger flap and fixed aerofoil nose, see Sketch 3.2a or 3.2b	m	ft
M	free-stream Mach number		
p	parameter in Equation (3.19) for K_Λ, see Equation (3.20)		
q	free-stream kinetic pressure	N/m^2	lbf/ft^2
R_c	aerofoil Reynolds number, based on free-stream conditions and c		
$R_{\bar{\bar{c}}}$	wing Reynolds number, based on free-stream conditions and $\bar{\bar{c}}$		
S	wing planform area, $2s\bar{c}$	m^2	ft^2
s	wing semi-span, see Sketch 1.1	m	ft
t	maximum thickness of aerofoil	m	ft
x_l	chordwise location of undeployed slat trailing edge, see Sketch 3.2a	m	ft
x_n	chordwise location of fixed aerofoil nose, see Sketch 3.2a	m	ft
x_τ	chordwise location of trailing edge of c_l' for deployed Krüger flaps and sealed slats, see Sketches 3.3a to 3.3c	m	ft
z_h	vertical location of hinge for drooped leading edge, see Sketch 3.1	m	ft
α	angle of attack	deg	deg
α_0	angle of attack for zero lift	deg	deg
δ_l, δ_l°	deflection of leading-edge device, positive leading edge down, see Sketches 3.1 to 3.3	rad, deg	rad, deg

ρ_l	leading-edge radius of basic (plain) aerofoil, see Sketches 3.1 to 3.3	m	ft
η	spanwise distance from wing centre-line as fraction of semi-span		
η_i	value of η at inboard limit of leading-edge device, see Sketch 1.1		
η_o	value of η at outboard limit of leading-edge device, see Sketch 1.1		
θ_l	angular parameter related to effective chord of leading-edge device, Equation (3.4)	rad	rad
Λ_0	wing leading-edge sweep angle, see Sketch 1.1	deg	deg
$\Lambda_{1/4}$	wing quarter-chord sweep angle, see Sketch 1.1	deg	deg
$\Lambda_{1/2}$	wing half-chord sweep angle, see Sketch 1.1	deg	deg
Λ_1	wing trailing-edge sweep angle, see Sketch 1.1	deg	deg
λ	wing taper ratio (tip chord/root chord)		

Subscripts

$(\ )_{expt}$	denotes experimental value
$(\ )_{pred}$	denotes predicted value

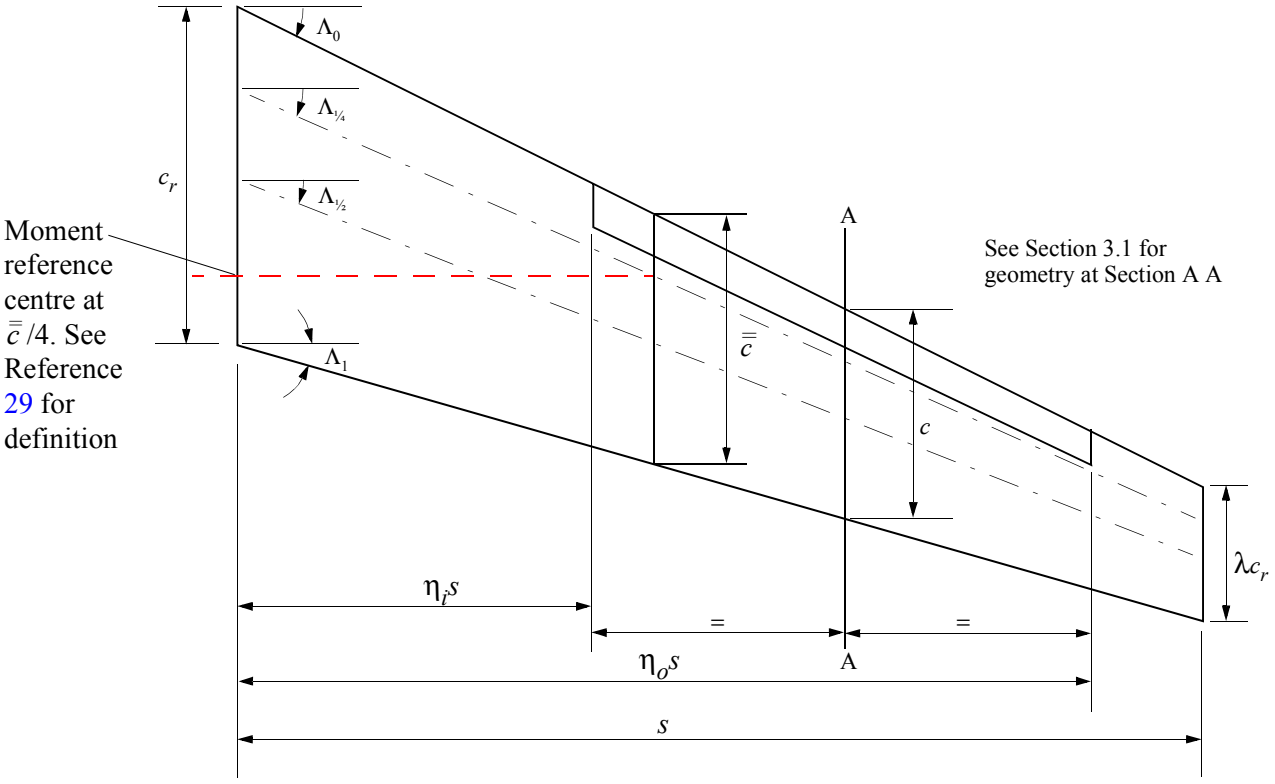

Sketch 1.1 Wing notation (leading-edge devices undeployed)

2. INTRODUCTION

This Item provides a method to obtain the increment in pitching moment coefficient at zero angle of attack due to deployment of various leading-edge devices at low speeds, either on an aerofoil or on a wing. The devices to be considered are listed in Table 3.1.

For aerofoils, the method predicts the centre of lift position, h_{2l}, due to leading-edge device deployment, based on the thin-aerofoil theory of Derivation 25 and modified to obtain correlation with the experimental data of Derivations 3, 5, 8, 9, 10, 14 and 21. This is combined with the increment in aerofoil lift coefficient, $\Delta C'_{L0l}$, calculated from Item No. 94027 (Derivation 2) to estimate the total pitching moment coefficient increment.

For wings with full-span leading-edge devices, factors dependent on planform geometry are applied to the pitching moment coefficient increment on a section that is representative of the wing, to allow for three-dimensional effects. Derivations 26 and 27 are used as the basis for these factors, with some adjustment to the simple theoretical assumptions. For wings with part-span devices, additional factors are introduced that are dependent on taper ratio, aspect ratio, sweep and spanwise extent of the device.

Section 3 describes the prediction method and Section 4 discusses Mach number and Reynolds number effects. The applicability and accuracy of the method are addressed in Section 5. The Derivation and References are given in Section 6. Section 7 provides worked examples illustrating the use of the Item for an aerofoil and a wing.

3. PREDICTION METHOD

The method for aerofoils requires the use of Item No. 94027 to determine the lift increment characteristics of the aerofoil/device combination from which to derive the pitching moment coefficient increment. All those parts of Item No. 94027 required in the estimation of $\Delta C'_{L0l}$ are included in this Item, in Section 3.1. It is therefore unnecessary to use Item No. 94027 unless background information is required. Section 3.1 also provides geometric definitions required in the determination of both $\Delta C'_{L0l}$ and h_{2l}.

For wings, the *streamwise* section, leading-edge device geometries and angles at the mid-span of the device are taken to be representative of the wing/device system, see Sketch 1.1. The method again requires the use of Item No. 94027 to determine the lift increment characteristics of the representative section from which to derive the section pitching moment coefficient increment. By this means the effects of spanwise variation are averaged out. Empirical corrections allow for the effects of wing planform geometry and the spanwise extent of the leading-edge devices.

3.1 Determination of $\Delta C'_{L0l}$

The increment in aerofoil lift coefficient at zero angle of attack, based on the extended chord length c', is given by

$$\Delta C'_{L0l} = [\Delta C'_{L0l}]_1 + [\Delta C'_{L0l}]_2 . \tag{3.1}$$

In Equation (3.1) the first term is the main contribution obtained from the theory, and is given by

$$[\Delta C'_{L0l}]_1 = K_0 a_l \delta_l , \tag{3.2}$$

where K_0 is an empirical correlation factor which is dependent upon the type of leading-edge device. The lift slope, a_l, is the theoretical rate of change of lift coefficient with respect to the deflection δ_l, positive nose down, given by thin-plate theory (Reference 25) as

$$a_l = -2(\theta_l - \sin\theta_l) \text{ rad}^{-1} \tag{3.3}$$

where $$\theta_l = \cos^{-1}(1 - 2c_{el}/c') \text{ rad} \tag{3.4}$$

and $$\sin\theta_l = [1 - (1-2c_{el}/c')^2]^{\frac{1}{2}}, \tag{3.5}$$

in which c_{el} is the effective chord of the leading-edge device.

Combination of Equations (3.1) to (3.5) gives

$$\Delta C'_{L0l} = -2K_0\,\delta_l\left\{\cos^{-1}(1 - 2c_{el}/c') - [1 - (1-2c_{el}/c')^2]^{\frac{1}{2}}\right\} + [\Delta C'_{L0l}]_2 , \tag{3.6}$$

in which $[\Delta C'_{L0l}]_2$ is a correction required only for slats and vented Krüger flaps.

The parameters involved in Equation (3.6) take different values according to the type of leading-edge device. Table 3.1 shows the source of the required geometry and definitions or locations whereby the relevant parameters can be determined.

TABLE 3.1 Source of geometry and relevant parameters required for evaluation of Equation (3.6) for various leading-edge devices

Leading-edge devices	*Geometry in*		*Parameters in Equation (3.6)*		
	Section	*Sketch*	c_{el}/c'	K_0	$[\Delta C'_{L0l}]_2$
Plain leading-edge flaps and drooped leading edges	3.1.1	3.1	c'_l/c'	1.0	0
Slats and vented Krüger flaps	3.1.2	3.2	c_l/c'	1.35	0.030
Krüger flaps and sealed slats	3.1.3	3.3	c'_l/c'	1.8	0

In addition to the sketches, Sections 3.1.1 to 3.1.3 contain special comments concerning the geometry and its influence on $\Delta C'_{L0l}$ via the correlation parameters.

3.1.1 Plain leading-edge flaps and drooped leading edges

Many variations in design are possible for plain leading-edge flows and drooped leading edges. Sketch 3.1 shows the specific case of a device deployed by rotation around a lower-surface hinge, for which

$$c_l' = c_l + z_h \tan(\delta_l/2) \tag{3.7}$$

and

$$c' = c + 2z_h \tan(\delta_l/2)\,. \tag{3.8}$$

The corresponding values of c_l' and c' appropriate to any other arrangement used would have to be determined.

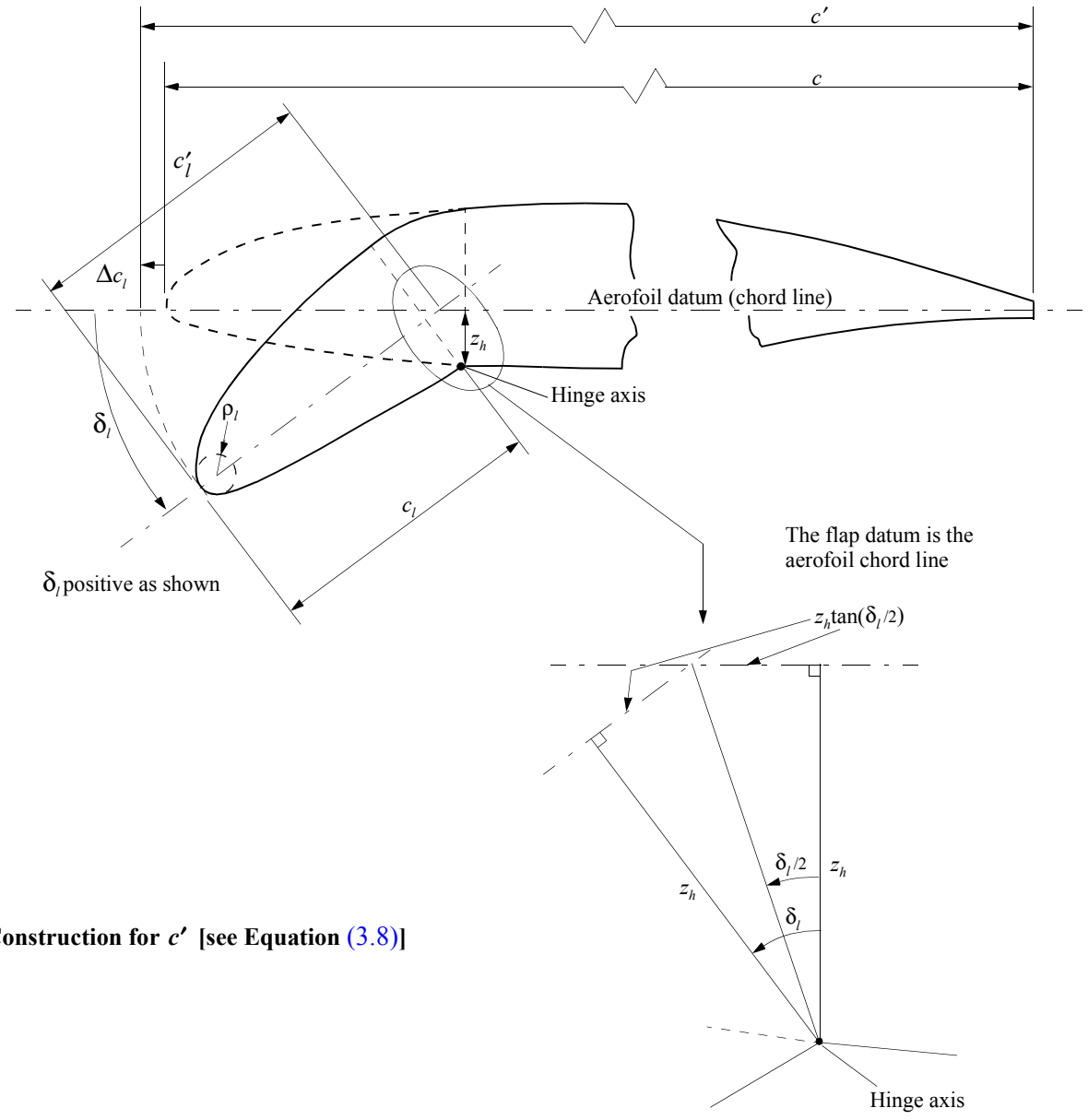

Construction for c' [see Equation (3.8)]

Sketch 3.1 Plain leading-edge flap and drooped leading edge

3.1.2 Slats and vented Krüger flaps

Geometric properties of slats and vented Krüger flaps are shown in Sketches 3.2a, 3.2b and 3.2c.

The deflection, δ_l, of both slats and vented Krüger flaps is defined using the angle between the datum chords of the slat (or flap) and the aerofoil. The slat (or flap) datum chord is defined as the line passing through the centre of the leading-edge radius and the slat (or flap) trailing edge. The extended chord, c', and the chord extension, Δc_l, are defined by rotating the slat (or flap) about the intersection of the slat (or flap) and aerofoil datum chords, as shown in Sketch 3.2c.

In Sketches 3.2a and 3.2b, for a slat and vented Krüger flap

$$c_l' = c_l - H_l \operatorname{cosec} \delta_l . \tag{3.9}$$

For a slat, the geometry in Sketch 3.2a and the construction in Sketch 3.2c give

$$\begin{aligned} c' &= c + \Delta c_l \\ &= c + c_l - x_n - L_l - b \\ &= c + c_l - x_n - L_l - H_l \tan(\delta_l / 2) . \end{aligned} \tag{3.10a}$$

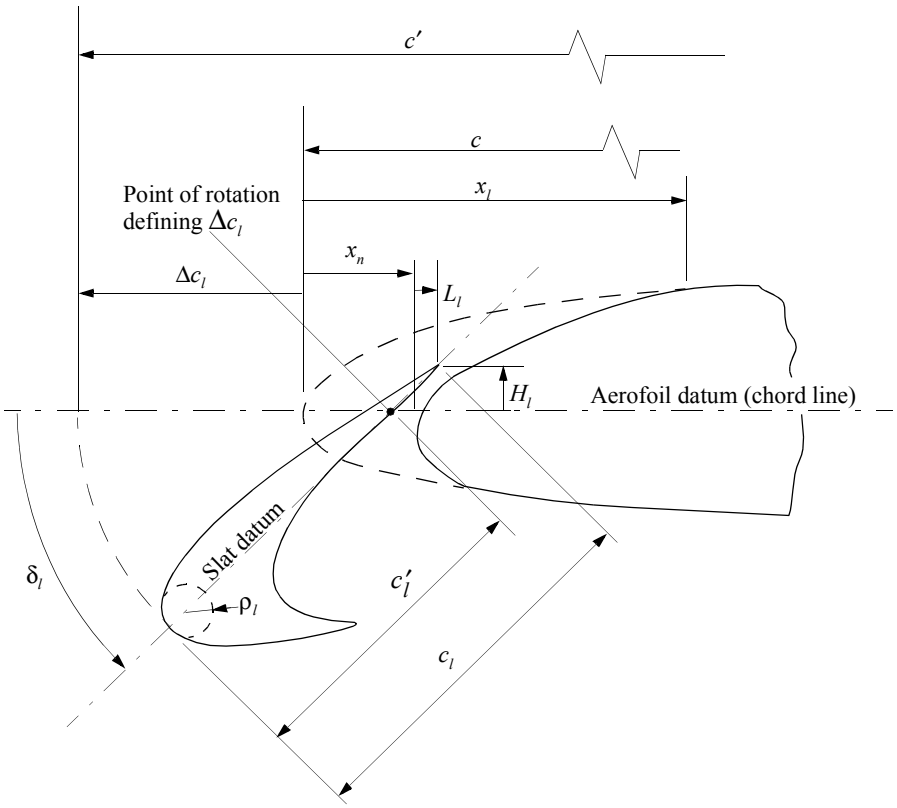

Construction for c' [see Equation (3.10a)]

δ_l, H_l and L_l positive as shown

Sketch 3.2a Slat

For a vented Krüger flap, the geometry in Sketch 3.2b and the construction in Sketch 3.2c give

$$\begin{aligned} c' &= c + \Delta c_l \\ &= c + c_l - L_l - b \\ &= c + c_l - L_l - H_l \tan(\delta_l/2) \ . \end{aligned} \tag{3.10b}$$

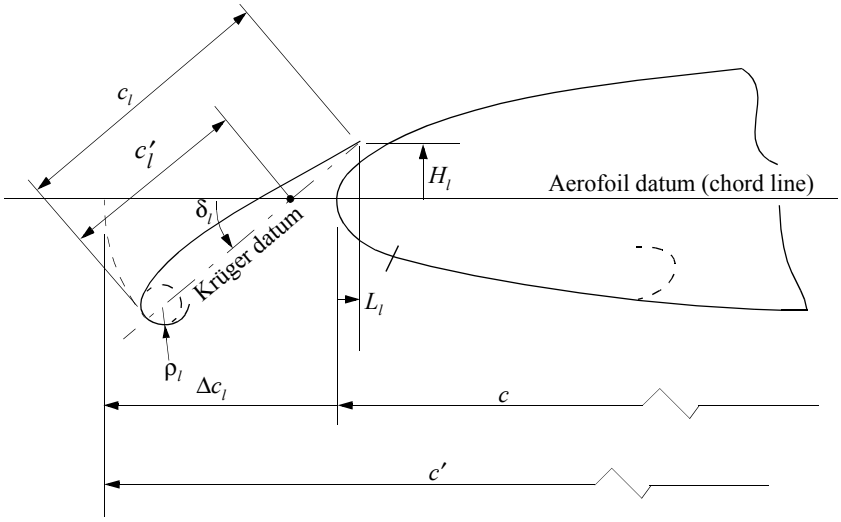

Construction for c' [see Equation (3.10b)]

Sketch 3.2b Vented Krüger flap

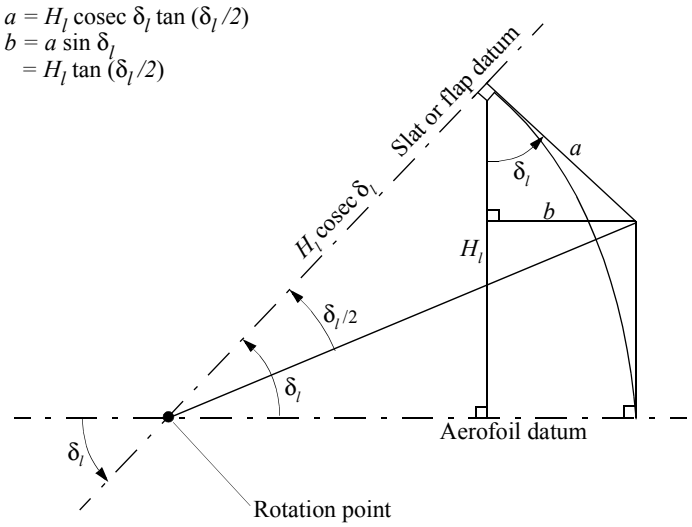

Sketch 3.2c Rotation of slat and vented Krüger flap

3.1.3 Krüger flaps and sealed slats

Krüger flaps and sealed slats have no slot and are therefore quite similar, in terms of their operation, to plain leading-edge flaps; the method for predicting $\Delta C'_{L0l}$ is likewise similar. Care is, however, required for the definition of equivalent flap chord c'_l and deflection angle δ_l. Sketches 3.3a to 3.3c show how they are defined for sealed slats and two forms of Krüger flap, termed upper and lower surface Krüger flaps.

For the sealed slat and upper-surface Krüger flap the equivalent leading-edge flap is taken to be related to that part of the aerofoil and flap forward of the point at which the section first departs from the original upper-surface profile due to the deployment of the flap, *i.e.* points A on Sketches 3.3a and 3.3b. The flap chord and deflection consistent with this are shown on those sketches. There is of necessity a small difference in the definitions for the case of the lower-surface Krüger flap, see Sketch 3.3c.

In Sketches 3.3a to 3.3c

$$\begin{aligned} c' &= c + \Delta c_l \\ &= c + c'_l - x_\tau . \end{aligned} \tag{3.11}$$

Sealed slats and upper-surface Krüger flaps (*Sketches 3.3a and 3.3b*)

For sealed slats and upper-surface Krüger flaps the values of c'_l and δ_l for the equivalent plain flap are obtained as follows. A straight line is drawn from the leading edge, passing through the centre of the flap leading-edge radius to point A, the point of departure from the original aerofoil surface. A circle centred on the mid-point of this line intersects the basic aerofoil chord at point B. The straight line joining B to the flap leading edge and passing through the centre of the flap leading-edge radius defines the equivalent plain flap chord c'_l. The angle between that chord and the aerofoil chord defines δ_l.

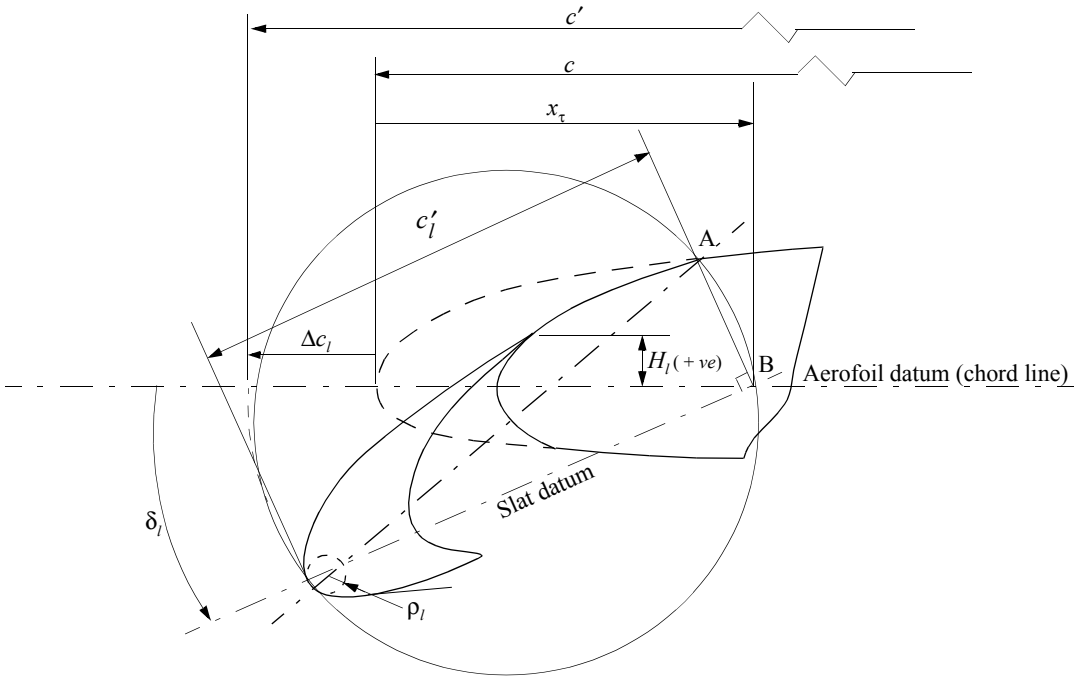

Construction for c' [see Equation (3.11)]

Sketch 3.3a Sealed slat

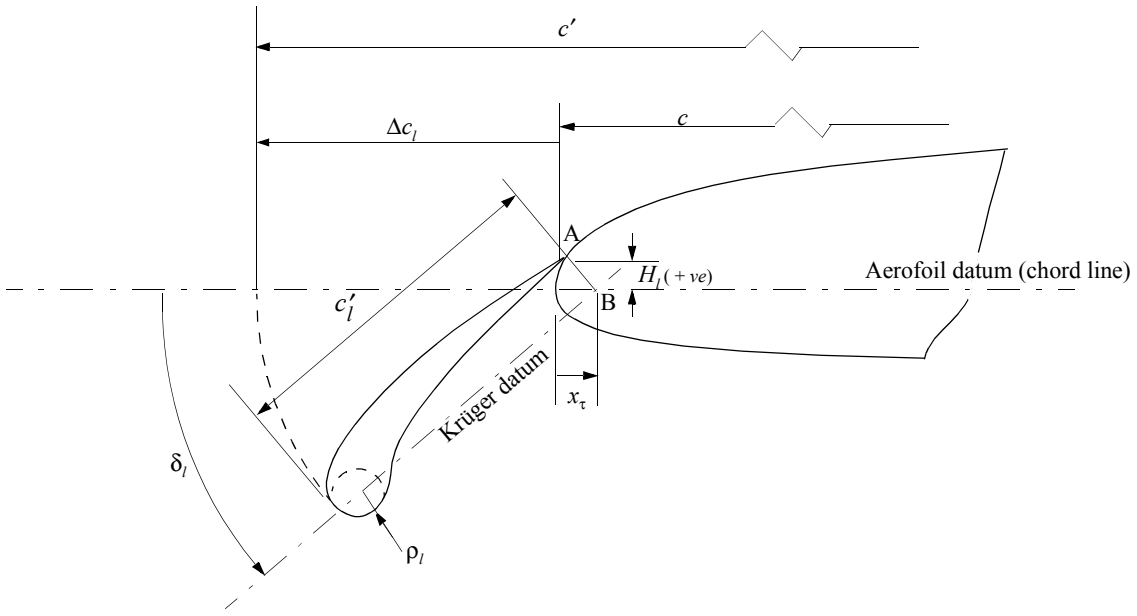

Construction for c' [see Equation (3.11)]

Sketch 3.3b Upper-surface Krüger flap

Lower-surface Krüger flap (*Sketch* 3.3c)

For a lower-surface Krüger flap, where the flap trailing-edge is on the aerofoil lower surface, the chord c'_l is taken as the length of the line drawn from A to the leading edge of the flap, passing through the centre of the flap leading-edge radius.

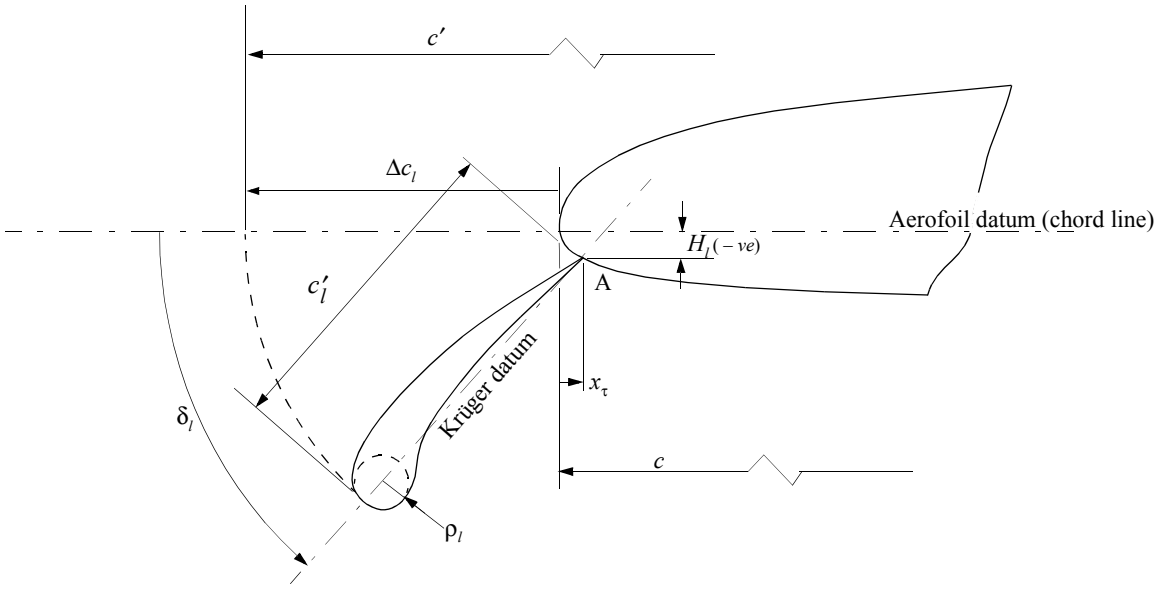

Construction for c' [see Equation (3.11)]

Sketch 3.3c Lower-surface Krüger flap

3.2 Aerofoil Pitching Moment Coefficient Increment $\Delta C_{ml\alpha 0}$

The increment in pitching moment coefficient at zero angle of attack, due to deployment of a leading-edge device on an aerofoil, is obtained from

$$\Delta C_{ml\alpha 0} = \Delta C'_{ml\alpha 0}(c'/c)^2 + 0.75\Delta C'_{L0l}(c'/c)(c'/c-1) + 0.75C_{L0}(c'/c-1) + C_{m\alpha 0}(c'/c-1)\,. \qquad (3.12)$$

Here, $\Delta C'_{ml\alpha 0}$ is the pitching moment coefficient at zero angle of attack due to deployment of a leading-edge device on an aerofoil, based on the extended chord, and is evaluated as

$$\Delta C'_{ml\alpha 0} = -\Delta C'_{L0l} h'_{2l}\,, \qquad (3.13)$$

C_{L0} is the lift coefficient of the basic aerofoil at zero angle of attack,

$C_{m\alpha 0}$ is the pitching moment coefficient of the basic aerofoil at zero angle of attack, referred to the quarter-chord point.

The middle two terms refer the moment to the quarter-chord point of the basic chord instead of the quarter-chord point of the extended chord.

The centre of the lift increment at zero angle of attack , h'_{2l}, is expressed as a fraction of the extended chord and measured positive aft from the quarter-chord point of the extended aerofoil chord. It is derived empirically from its theoretical value in Derivation 25 for a hinged plate on a thin aerofoil, adjusted to allow for chord extension by replacing c_l/c with c'_l/c' to give

$$h'_{2lT} = \frac{-0.25[1-(1-2c'_l/c')^2]^{1/2}[1-(1-2c'_l/c')]}{\left\{\cos^{-1}(1-2c'_l/c') - [1-(1-2c'_l/c')^2]^{1/2}\right\}}\,. \qquad (3.14a)$$

Values of h'_{2lT} determined from Equation (3.14a) are given in Figure 1 as a function of c'_l/c', and over the range $0 \le c'_l/c' \le 0.5$ can be approximated as

$$h'_{2lT} = 0.62c'_l/c' - 0.75\,. \qquad (3.14b)$$

A factor to obtain correlation with the experimental data in Derivations 3, 5, 8, 9, 10, 14 and 21 gives

$$h'_{2l} = K_m\, h'_{2lT}\,, \qquad (3.15)$$

where K_m is dependent on the type of leading-edge device, as shown in Table 3.2.

The final terms in Equation (3.12) involving C_{L0} and $C_{m\alpha 0}$, the lift and pitching moment coefficients at zero angle of attack for the basic aerofoil, provide an approximation to the effect of extension of the aerofoil without device angular rotation. The term involving $C_{m\alpha 0}$ is always small compared to the first two terms in Equation (3.12) and it is sufficient to replace $C_{m\alpha 0}$ by C_{m0}, the pitching moment coefficient of the basic aerofoil at zero lift. The approximation is exact for all cases in which the aerodynamic centre is at the quarter-chord point.

The method in Item No. 72024 (Reference 28) may be used to evaluate C_{m0i}, the inviscid value of C_{m0}, and Figure 1 of Item No. 87001 (Reference 30) provides a viscous correction factor F, so that

$$C_{m0} = FC_{m0i}. \tag{3.16}$$

A good approximation to F is

$$F = 1 - 0.29\left[\sin\left(\frac{-C_{m0i}}{0.29}\frac{\pi}{2}\right)\right]^{0.7}, \text{ where the angle is measured in radians.} \tag{3.17}$$

The method must not be used to obtain pitching moment increments due to extension without rotation, since those values are critically dependent on detailed geometry not accounted for in this method. See Table 5.2 for the minimum validated device deflection angles.

3.3 Wing Pitching Moment Coefficient Increment $\Delta C_{mlw\alpha 0}$

For a wing at zero angle of attack the increment in pitching moment coefficient due to leading-edge device deployment is

$$\Delta C_{mlw\alpha 0} = K_l(K_o - K_i)\Delta C_{ml\alpha 0} + K_{l\Lambda}(K_{\Lambda o} - K_{\Lambda i})(A/2)\Delta C'_{L0l}\,(c'/c)\tan\Lambda_{1/4}, \tag{3.18}$$

where A is the wing aspect ratio, $\Lambda_{1/4}$ is the wing quarter-chord sweep angle, and $\Delta C'_{L0l}$ and $\Delta C_{ml\alpha 0}$ are now calculated from Equations (3.6) and (3.12), respectively, for the representative streamwise section of the wing, taken at device mid-span.

The part-span factors K_i and K_o are obtained from Figure 2 as functions of wing taper ratio and the inboard and outboard limits of the leading-edge device, $\eta = \eta_i$ and η_o, respectively.

The correlation factors K_l and $K_{l\Lambda}$ for leading-edge devices have been derived from the data of Derivations 4, 6, 7, 11 to 13, 15 to 20, 22 to 24 and take different values according to the type of device, as shown in Table 3.2.

TABLE 3.2 Values of K_m required for evaluation of Equation (3.15) and of K_l and $K_{l\Lambda}$ required for evaluation of Equation (3.18)

Leading-edge device	K_m	K_l	$K_{l\Lambda}$
Plain leading-edge flaps and drooped leading edges	1.05	$\cos\delta_l^\circ$	1
Slats and vented Krüger flaps	1.0	$1.1\cos\delta_l^\circ\cos\Lambda_0$	1
Krüger flaps and sealed slats	0.7	$1.15\cos\delta_l^\circ\cos\Lambda_0$	1

The part-span wing-sweep factors, $K_{\Lambda i}$ and $K_{\Lambda o}$, are obtained for leading-edge devices from Figures 3a to 3f as functions of the extended chord ratio, c'/c, and the inboard and outboard limits of the device, $\eta = \eta_i$ and η_o, respectively, for a range of values of wing taper ratio. Note that for all cases with a full-span device or an unswept quarter-chord line the second term in Equation (3.18) has a value of zero.

The data for K_Λ, taken to be applicable to leading-edge devices, are given in Figures 3a to 3f for $\lambda = 0$, 0.1, 0.2, 0.4, 0.6 and 1, and were obtained from Derivation 26 for extended flaps in the form

$$K_\Lambda = \frac{-3(1+\lambda)}{4(1+\lambda+\lambda^2)}\left\{\left[0.5\eta^2 - 0.333(1-\lambda)\eta^3\right]\left[(c'/c)(1-p)+p\right] - \left[0.5 - 0.333(1-\lambda)\right]p\right\}, \qquad (3.19)$$

where

λ is the wing taper ratio

and

$$p = \frac{(c'/c)[\eta - 0.5(1-\lambda)\eta^2]}{0.5(1+\lambda) - [\eta - 0.5(1-\lambda)\eta^2](1-c'/c)}. \qquad (3.20)$$

4. EFFECTS OF MACH NUMBER AND REYNOLDS NUMBER

4.1 Mach Number Effects

High local Mach numbers will occur at low free-stream Mach number as a result of high-angle deployment of leading-edge devices. Significant Mach number effects will occur at free-stream Mach numbers greater than about 0.2 at large values of δ_l°, and at progressively smaller values of this angle as Mach number is increased. None of the data considered for this Item was for a Mach number greater than 0.21.

4.2 Reynolds Number Effects

For the data used in the derivation of this Item no effect of Reynolds number on $\Delta C_{ml\alpha 0}$ or $\Delta C_{mlw\alpha 0}$ was found over the ranges of Reynolds number shown in Tables 5.1 and 5.2.

5. APPLICABILITY AND ACCURACY

5.1 Applicability

5.1.1 Aerofoils

The method given in this Item for estimating the position of the centre of the lift increment and the increment in pitching moment coefficient at zero angle of attack due to deployment of a leading-edge device applies only to aerofoils without the deployment of a trailing-edge flap. Combined deployment will be covered in a future Item. Simple addition of the contributions from leading-edge devices and trailing-edge flaps is invalid if there is any chord extension.

Table 5.1 summarises the parameter ranges covered by the experimental data and correlated by Equations (3.12) to (3.15).

TABLE 5.1 Parameter ranges for test data for leading-edge devices on aerofoils used in method of Section 3.2

Parameter	*Ranges for:*		
	Plain leading-edge flaps and drooped leading edges	*Slats and vented Krüger flaps*	*Krüger flaps and sealed slats*
t/c	0.04 to 0.10	0.09 to 0.12	0.09 to 0.12
c_l/c	0.15 to 0.16	0.14 to 0.175	0.10 to 0.12
c'/c	1.0 to 1.03	1.1 to 1.123	1.09 to 1.1
H_l/c	Not applicable	–0.007 to 0.045	–0.02 to 0.0173
L_l/c	Not applicable	0 to 0.013	Not applicable
x_n/c	Not applicable	0.02 to 0.048	Not applicable
x_τ/c	Not applicable	Not applicable	0.005 to 0.026
z_h/c	0.005 to 0.038	Not applicable	Not applicable
δ_l°	5º to 45º	34º to 44º	32º to 52º
$R_c \times 10^{-6}$	5.8 to 6.0	2.2 to 6.0	6.0
M	0.1 to 0.17	0.17	0.11 to 0.12

The method is expected to apply to the more extensive ranges of geometries covered by Table 5.1 in Item No. 94027.

5.1.2 Wings

The method given in this Item for estimating the increment in pitching moment coefficient, at zero angle of attack, due to deployment of a leading-edge device on a wing, has been shown to be applicable to straight-tapered wings covering a wide range of planform parameters. Table 5.2 summarises the parameter ranges covered by the experimental data that were used in the development of the method.

If there is a large or irregular variation in c_l/c, the device should be divided into two or more spanwise panels. A calculation is then made separately for each panel, using its mid-span geometry, and the results are summed to provide a total value of $\Delta C_{mlw\alpha 0}$.

No wings with cranked leading or trailing edges or curved tips were included in the analysis. It is suggested that for such wings the planform parameters λ and $\Lambda_{1/4}$ be calculated for the equivalent straight-tapered planform as defined in Item No. 76003 (Reference 29). Care should be taken with the definition of c_l/c and the user of the final result should always be aware that the method has not been validated for such wings.

The method, as it stands, has only been validated for wings without trailing-edge flaps. Combined deployment of leading-edge devices and trailing-edge flaps will be covered in a future Item. See comments in Section 5.1.1.

TABLE 5.2 Parameter ranges for test data for leading-edge devices on wings used in method of Section 3.3

Parameter	*Ranges for:*		
	Plain leading-edge flaps and drooped leading edges	*Slats and vented Krüger flaps*	*Krüger flaps and sealed slats*
A	2.29 to 6.0	3.78 to 8.35	2.88 to 8.0
λ	0.38 to 1	0.35 to 1	0.31 to 1
Λ_0	0 to 52º	0 to 49º	0 to 52º
Λ_1	0 to 45º	0 to 42º	0 to 45º
$A\tan\Lambda_0$	0 to 5.6	0 to 4.5	0 to 8.4
$A\tan\Lambda_{½}$	0 to 4.7	0 to 4.0	0 to 7.6
η_i	0 to 0.6	0 to 0.75	0 to 0.7
η_o	0.95 to 1	0.95 to 1	0.95 to 1
t/c	0.045 to 0.10	0.06 to 0.12	0.06 to 0.12
c_l/c	0.13 to 0.20	0.12 to 0.22	0.10 to 0.24
c'/c	1.0 to 1.04	1.06 to 1.17	1.10 to 1.23
δ_l°	2º to 40º	14º to 41º	29º to 63º
$R_{\bar{c}} \times 10^{-6}$	2.0 to 6.8	1.7 to 6.8	2.9 to 6.8
M	≤ 0.20	≤ 0.21	≤ 0.19

5.2 Accuracy

5.2.1 Aerofoils

Sketch 5.1 shows the comparison between predicted and experimental values of pitching moment coefficient increments at zero angle of attack due to deployment of various leading-edge devices on an aerofoil. The experimental data were obtained from Derivations 3, 5, 8, 9, 10, 14 and 21; the rms error is 0.0046 and 80% of the data are correlated to within ±0.005.

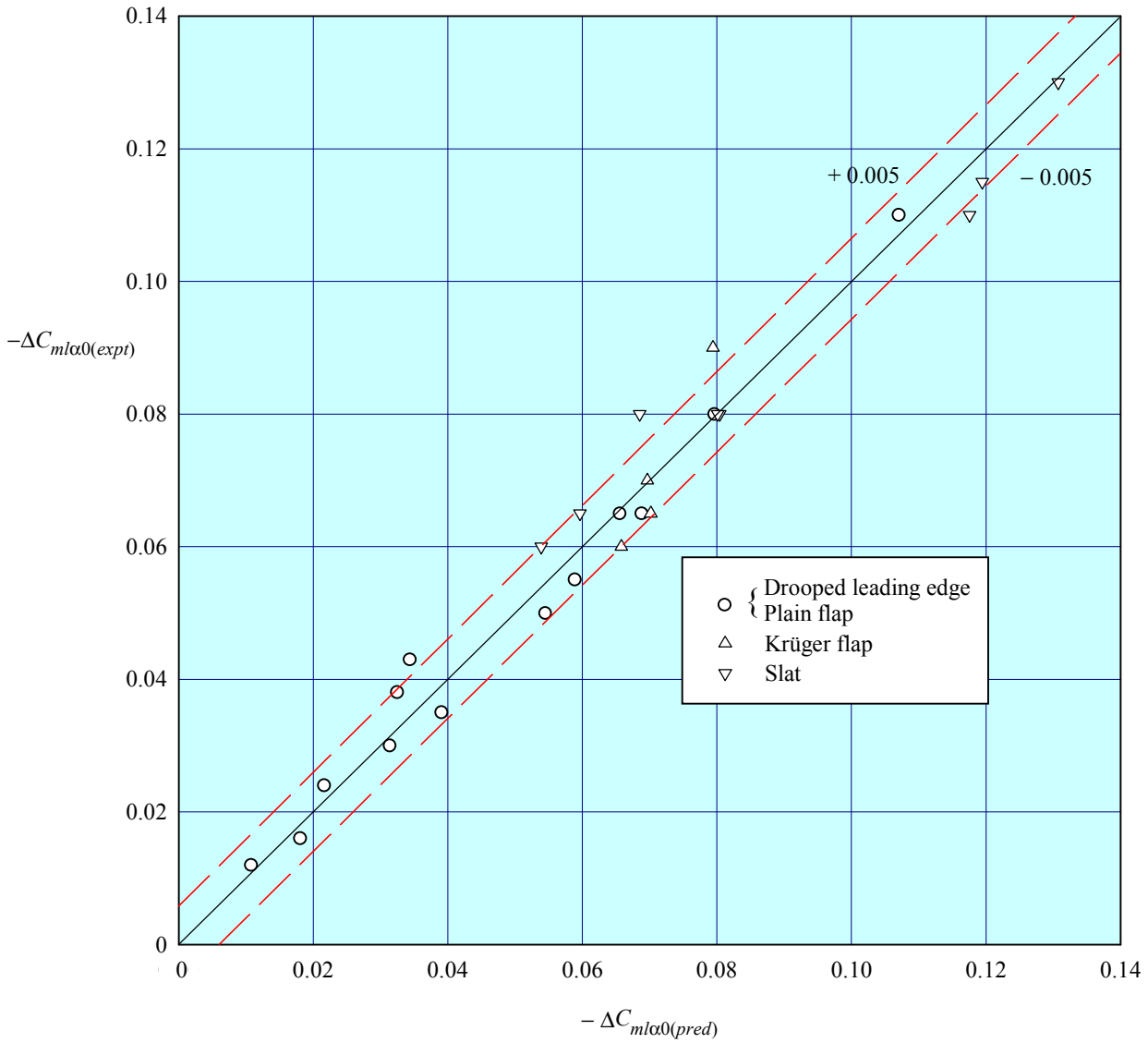

Sketch 5.1 Comparison of predicted and experimental values of $\Delta C_{ml\alpha 0}$ for deployment of leading-edge devices on aerofoils

5.2.2 Wings

The comparison between predicted and experimental values of the pitching moment coefficient increment, $\Delta C_{mlw\alpha 0}$, due to deployment of both full-span and part-span leading-edge devices is shown on Sketch 5.2 for wings, for data from Derivations 4, 6, 7, 11 to 13, 15 to 20, 22 to 24; the rms error is 0.0050 and 95% of the data are correlated to within ±0.010.

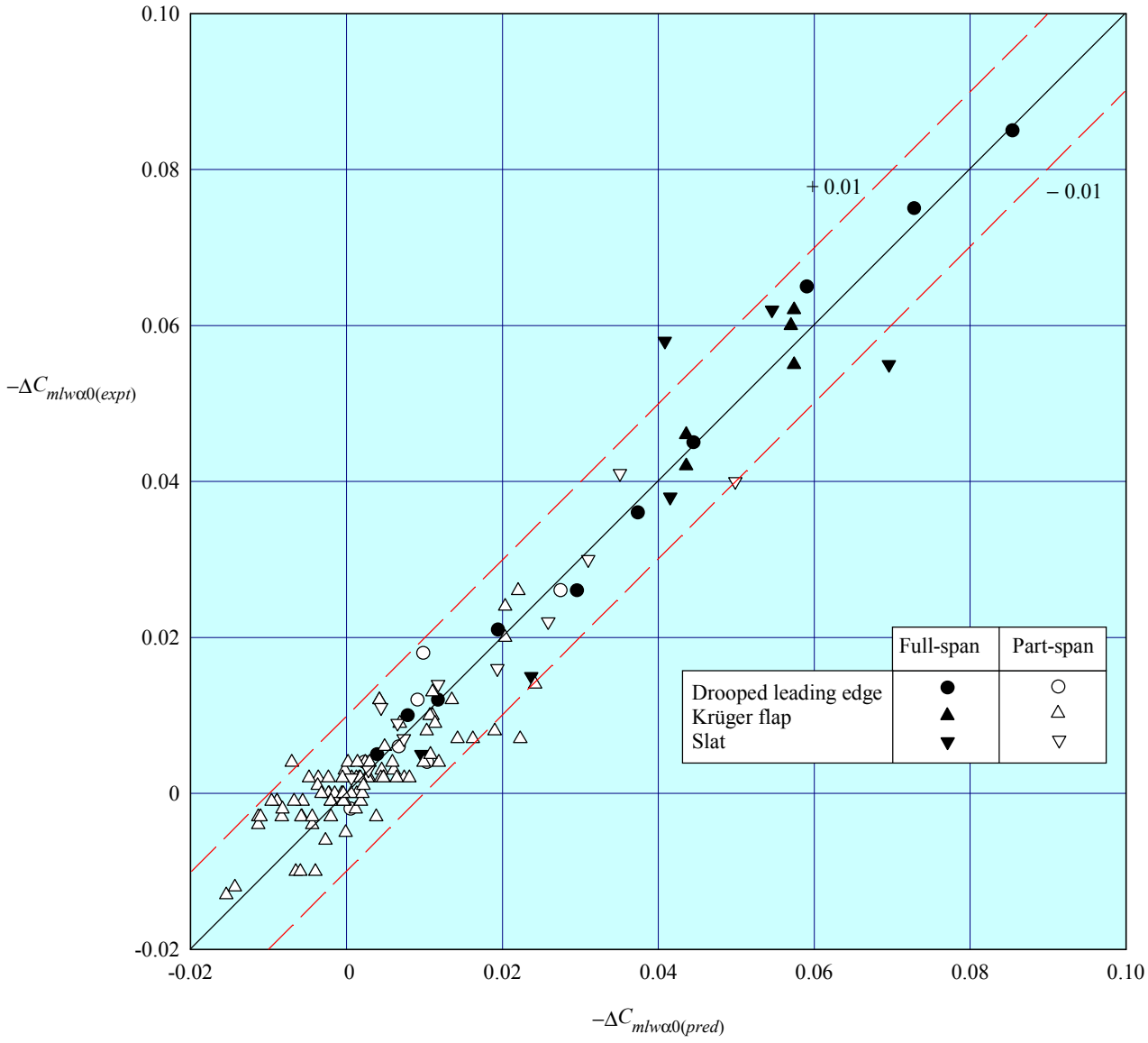

Sketch 5.2 Comparison of predicted and experimental values of $\Delta C_{mlw\alpha 0}$ for deployment of leading-edge devices on wings

6. DERIVATION AND REFERENCES

6.1 Derivation

The Derivation lists selected sources of information that have been used in the preparation of this Item.

6.1.1 ESDU Data Items

1. ESDU — Slope of lift curve for two-dimensional flow.
ESDU International, Item No. Wings 01.01.05, 1955.

2. ESDU — Increments in aerofoil lift coefficient at zero angle of attack and in maximum lift coefficient due to deployment of various leading-edge high-lift devices at low speeds.
ESDU International, Item No. 94027, 1994.

6.1.2 Wind-tunnel test reports

3. SCHULDENFREI, M.J. — Wind-tunnel investigation of an NACA 23012 airfoil with a Handley Page slat and two flap arrangements.
NACA WR L-261, 1942.

4. BLACKBURN AIRCRAFT — Wind tunnel tests on moderately large chord flaps with single and multiple slots.
Blackburn Aircraft Limited, Report W.T. 85/42, 1943.

5. FULLMER, F.F. — Two-dimensional wind-tunnel investigation of an NACA 64-012 airfoil equipped with two types of leading-edge flap.
NACA tech. Note 1277, 1947.

6. CONNER, D.W.
NEELY, R.H. — Effects of a fuselage and various stall control flaps on aerodynamic characteristics in pitch of a NACA 64-series 40º sweptback wing.
NACA RM L6L27 (TIL 1375), 1947.

7. GRAHAM, R.R. — Investigation of high-lift and stall control devices on a NACA 64-series 42º sweptback wing with and without a fuselage.
NACA RM L7G09 (TIL 1407), 1947.

8. NUBER, R.J.
GOTTLIEB, S.M. — Two-dimensional wind-tunnel investigation at high Reynolds numbers of an NACA 65A006 airfoil with high-lift devices.
NACA RM L7K06 (TIL 1569), 1948.

9. FULLMER, F.F. — Two-dimensional wind-tunnel investigation of an NACA 64-009 airfoil equipped with two types of leading-edge flap.
NACA tech. Note 1624, 1948.

10. ROSE, L.M.
ALTMAN, J.M. — Low speed experimental investigation of a thin, faired, double-wedge airfoil section with nose and trailing-edge flaps.
NACA tech. Note 1934, 1949.

11. KOVEN, W.
GRAHAM, R.R. — Wind-tunnel investigation of high lift and stall control devices on a 37º sweptback wing of aspect ratio 6.
NACA RM L8D29 (TIL 1907), 1948.

12. LANGE, R.H.
MAY, R.W.
Effect of leading-edge high-lift devices and split flaps on the maximum lift and lateral characteristics of a rectangular wing of aspect ratio 3.4 with circular arc airfoil sections at Reynolds numbers from 2.9×10^6 to 8.4×10^6.
NACA RM L8D30 (TIL 1971), 1948.

13. SCHNEITER, L.E.
VOGLER, R.D.
Wind tunnel investigation at low speeds of various plug aileron and lift flap configurations on 42º sweptback semi-span wing.
NACA RM L8K19 (TIL 2058), 1948.

14. GOTTLIEB, S.M.
Two-dimensional wind-tunnel investigation of two NACA airfoils with leading-edge slats.
NACA RM L8K22 (TIL 1891), 1949.

15. PASAMANICK, J.
SELLERS, T.B.
Low speed investigation of leading-edge and trailing-edge flaps on a 47.5º swept-back wing of aspect ratio 3.4 at a Reynolds number of 4.4×10^6.
NACA RM L50E02 (TIL 2404), 1950.

16. SALMI, R.J.
Effects of leading-edge devices and trailing-edge flaps on longitudinal characteristics of two 47.7º sweptback wings of aspect ratio 5.1 and 6 at a Reynolds number of 6.0×10^6.
NACA RM L50F20 (TIL 2446), 1950.

17. GRINER, R.F.
FOSTER, G.V.
Low-speed longitudinal and wake air-flow characteristics at a Reynolds number of 6.0×10^6 of a 52º sweptback wing equipped with various spans of leading-edge flaps, a fuselage, and a horizontal tail at various vertical positions.
NACA RM L51C30 (TIL 2790), 1951.

18. LIPSON, S.
BARNETT, U.R.
Force and pressure investigation at large scale of a 49º sweptback semispan wing having NACA 65A006 sections and equipped with various slat arrangements.
NACA RM L51K26 (TIL 3001), 1952.

19. PRATT, G.L.
SHEILDS, R.R.
Low speed longitudinal characteristics of a 45º sweptback wing of aspect ratio 8 with high-lift and stall control devices at Reynolds numbers from 1,500,400 to 4,800,000.
NACA RM L51J04 (TIL 3038), 1952.

20. BARNETT, U.R.
LIPSON, S.
Effects of several high-lift and stall-control devices on the aerodynamic characteristics of a semispan 49º sweptback wing.
NACA RM L52D17a (TIL 3326), 1952.

21. KELLY, J.A.
Lift and pitching moment at low speeds of the NACA 64A010 airfoil section equipped with various combinations of a leading-edge slat, leading-edge flap, split flap and double-slotted flap.
NACA tech. Note 3007, 1953.

22. BUTLER, S.F.J.
GUYETT, M.B.
Low-speed wind-tunnel tests on a delta-wing aircraft model (S.R. 177), with blowing over the trailing-edge flaps and ailerons.
RAE Report No. Aero 2671, 1962.

23. LOVELL, D.A.
A wind tunnel investigation of the effects of flap span and deflection angle, wing planform and a body on the high lift performance of a 28º swept wing.
RAE TR 76030, 1976.

24. RAE
Unpublished data, 1981.

6.1.3 Theory

25. GLAUERT, H. — Theoretical relationships for an aerofoil with hinged flap. ARC R&M 1095, 1927.

26. DENT, M.M. CURTIS, M.F. — A method of estimating the effect of flaps on pitching moment and lift on tailless aircraft. RAE Report No. Aero 1861, 1943.

27. YOUNG, A.D. — The aerodynamic characteristics of flaps. ARC R&M 2622 (RAE Report No. Aero 2185), 1947.

6.2 References

The References are sources of information supplementary to those used in the derivation of this Item.

28. ESDU — Aerodynamic characteristics of aerofoils in compressible inviscid airflow at subcritical Mach numbers. ESDU International, Item No. 72024, 1972.

29. ESDU — Geometrical properties of cranked and straight tapered wing planforms. ESDU International, Item No. 76003, 1976.

30. ESDU — Wing pitching moment at zero lift at subcritical Mach numbers. ESDU International, Item No. 87001, 1987.

31. ESDU — Slope of aerofoil lift curve for subsonic two-dimensional flow. ESDU International, Item No. 97020, 1997.

32. ESDU — Aerofoil incidence for zero lift in subsonic two-dimensional flow. ESDU International, Item No. 98011, 1998.

7. EXAMPLES

7.1 Example 1: Pitching Moment Increment due to a Leading-edge Slat on an Aerofoil

Estimate the increment in pitching moment coefficient at zero angle of attack due to the deployment of a 15% chord leading-edge slat ($x_l = 0.15c$) installed on a modified NACA 65_2-215 section as shown in Sketch 7.1. The modifications produced a linear profile rearwards from 75% chord and 65% chord on the upper and lower surfaces, respectively. Boundary-layer transition may be assumed to occur at the leading edge.

The required geometrical parameters are as follows.

$$c_l/c = 0.164\,,\ \delta_l^\circ = 35°\ \ (\delta_l = 0.611\ \text{rad}),$$
$$x_n/c = 0.04\,,\ H_l/c = 0.02\,,\ L_l/c = 0$$

The flow conditions are $M = 0.2$ and $R_c = 4.5 \times 10^6$, both of which are within the ranges of application of the method. Although the aerofoil thickness, $t/c = 0.15$, is slightly outside the range of Table 5.1, the method is likely to remain reliable since this value was included in the range of t/c used to derive the method for $\Delta C'_{L0l}$ in Item No. 94027.

The inviscid value, C_{m0i}, of the pitching moment coefficient for aerofoil zero lift, may be calculated by the method in Item No. 72024 (Reference 28) and is taken as – 0.031 for $M = 0.2$.

The angle of attack for zero lift may be calculated by the method in Item No. 98011 (Reference 32) and is taken as –1.004° for the given flow conditions.

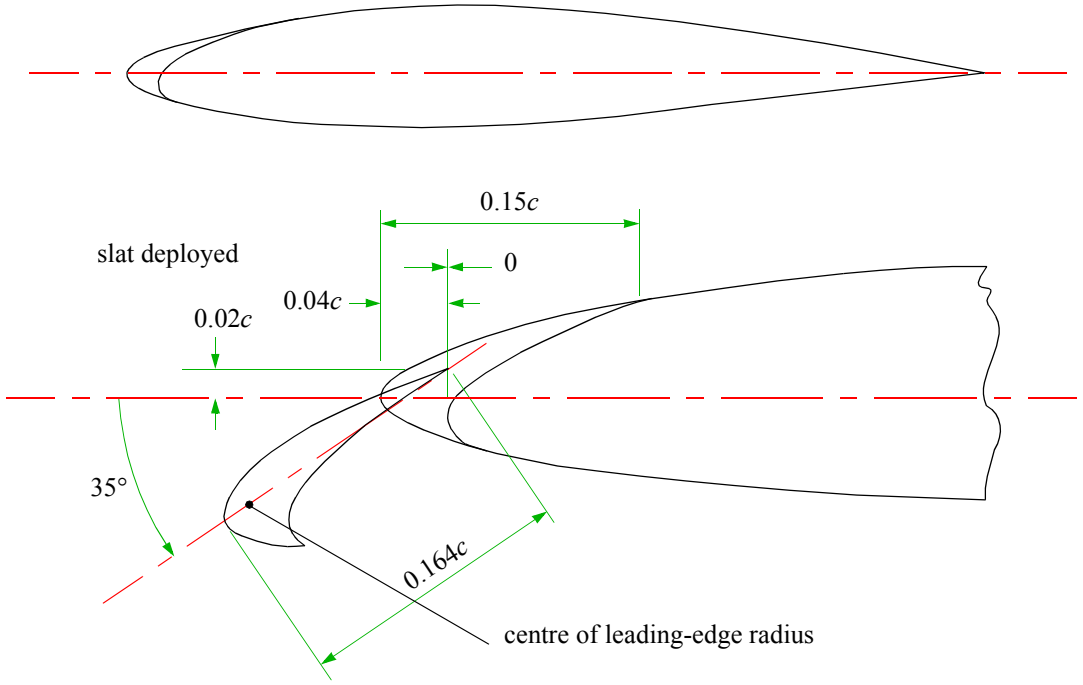

Sketch 7.1 Aerofoil and slat geometry

(1) Obtain C_{L0} and $C_{m\alpha 0}$

For the modified NACA 65_2–215 section, Item No. W.01.01.05 (Derivation 1) is used with boundary-layer transition at the leading edge to give

$$(a_1)_0 = 5.62 \text{ rad}^{-1} .$$

(Although a more accurate estimate of the lift-curve slope is available by the method of Item No. 97020 (Reference 31), the value from Item No. Wings 01.01.05 is used because the method of that Item is employed in other worked examples in the group of Items on high-lift device deployment.)

The angle of attack for zero lift is given as $\alpha_0 = -1.004°$. Now

$$C_L = (a_1)_0(\alpha - \alpha_0)/57.3 ,$$

so that with $\alpha = 0$

$$C_{L0} = 5.62 \times (1.004 / 57.3) = 0.0985 .$$

As remarked in Section 3.2, the term in Equation (3.12) involving $C_{m\alpha 0}$ is always small compared with the first two terms so that it is acceptable to assume that for the basic aerofoil the pitching moment coefficient at zero angle of attack is equal to the pitching moment coefficient at zero lift, *i.e.* $C_{m\alpha 0} \approx C_{m0}$.

From Equation (3.16),

$$C_{m0} = FC_{m0i} .$$

The inviscid value C_{m0i} is taken as -0.031 and the viscous correction factor F is given by Equation (3.17),

$$F = 1 - 0.29\left[\sin\left(\frac{-C_{m0i}}{0.29}\frac{\pi}{2}\right)\right]^{0.7} , \text{ where the angle is measured in radians,}$$

so that

$$F = 1 - 0.29\left[\sin\left(\frac{0.031}{0.29}\frac{\pi}{2}\right)\right]^{0.7}$$

$$= 0.917 .$$

Thus $C_{m\alpha 0} \approx C_{m0} = 0.917 \times (-0.031) = -0.028$.

(2) Obtain c'/c, c'_l/c' and c_{el}/c'

Table 3.1 shows that Section 3.1.2 is the relevant one giving the geometry for the slat.

Equation (3.10a) gives the extended chord of an aerofoil with a slat as

$$c' = c + c_l - x_n - L_l - H_l \tan(\delta_l/2)$$

so that $$c'/c = 1 + 0.164 - 0.04 - 0 - 0.02 \tan(0.611/2)$$
$$= 1.118.$$

Equation (3.9) gives

$$c'_l = c_l - H_l \operatorname{cosec} \delta_l$$

so that $$c'_l/c = 0.164 - 0.02 \operatorname{cosec}(0.611)$$
$$= 0.129,$$

and $$c'_l/c' = 0.129/1.118$$
$$= 0.115.$$

Table 3.1 shows that the value of c_{el} is taken as c_l for a slat, *i.e.*

$$c_{el}/c = c_l/c = 0.164,$$
$$c_{el}/c' = c_l/c' = 0.164/1.118$$
$$= 0.147.$$

(3) Determine $\Delta C'_{L0l}$

From Table 3.1, $K_0 = 1.35$ and $[\Delta C'_{L0l}]_2 = 0.030$.

Equation (3.6) gives

$$\Delta C'_{L0l} = -2K_0\delta_l\left\{\cos^{-1}(1-2c_{el}/c') - [1-(1-2c_{el}/c')^2]^{1/2}\right\} + [\Delta C'_{L0l}]_2$$

$$= -2 \times 1.35 \times 0.611 \times \left\{\cos^{-1}(1-2\times 0.147) - [1-(1-2\times 0.147)^2]^{1/2}\right\} + 0.030$$

$$= -0.100.$$

(4) **Determine h'_{2l}**

From the approximation given by Equation (3.14b),

$$h'_{2lT} = 0.62c'_l/c' - 0.75 = 0.62 \times 0.115 - 0.75 = -0.679.$$

This compares with the exact value – 0.681 generated by Equation (3.14a). See also Figure 1.

Table 3.2 gives $K_m = 1.0$ for a slat.

From Equation (3.15),

$$\begin{aligned} h'_{2l} &= K_m h'_{2lT} \\ &= 1.0 \times (-0.679) \\ &= -0.679. \end{aligned}$$

(5) Determine $\Delta C_{ml\alpha 0}$

From Equation (3.13),

$$\begin{aligned} \Delta C'_{ml\alpha 0} &= -\Delta C'_{L0l} h'_{2l} \\ &= -(-0.100 \times -0.679) \\ &= -0.0679. \end{aligned}$$

From Equation (3.12),

$$\begin{aligned} \Delta C_{ml\alpha 0} &= \Delta C'_{ml\alpha 0}(c'/c)^2 + 0.75\Delta C'_{L0l}(c'/c)(c'/c-1) + 0.75C_{L0}(c'/c-1) + C_{m\alpha 0}(c'/c-1) \\ &= (-0.0679) \times 1.118^2 + 0.75 \times (-0.100) \times 1.118 \times (1.118-1) + 0.75 \times 0.0985 \times (1.118-1) \\ &\qquad + (-0.028) \times (1.118-1) \\ &= -0.0849 - 0.0099 + 0.0087 - 0.0033 \\ &= \mathbf{-0.0894}. \end{aligned}$$

7.2 Example 2: Pitching Moment Increment due to a Leading-edge Slat on a Wing

Estimate the increment in pitching moment coefficient at zero angle of attack for a Reynolds number $R_{\bar{\bar{c}}} = 4.5 \times 10^6$ and a free-stream Mach number $M = 0.2$ for a wing with a part-span 15% chord slat that extends from 30% of the wing semi-span to the wing tip, as shown in Sketch 7.2. The wing has the planform parameter values

$$A = 8, \Lambda_{1/4} = 25° \text{ and } \lambda = 0.4$$

and across the whole span the streamwise section is the modified NACA 65_2–215 profile which was used in Example 1.

When deployed, the streamwise section geometry and deflection angle of the slat at its mid-span are as shown in Sketch 7.1.

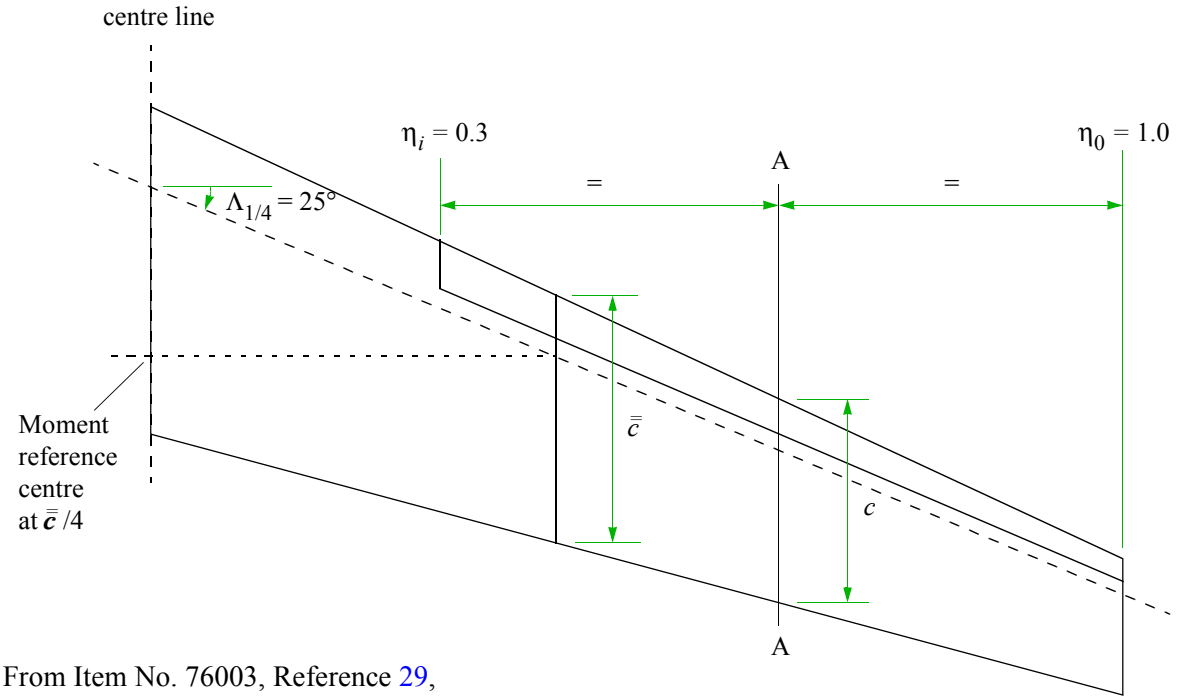

From Item No. 76003, Reference 29,

$$\Lambda_0 = \tan^{-1}\left(\tan\Lambda_{1/4} + \frac{1}{A}\frac{1-\lambda}{1+\lambda}\right) = 27.47°,$$

$$\Lambda_1 = \tan^{-1}\left(\tan\Lambda_{1/4} - \frac{3}{A}\frac{1-\lambda}{1+\lambda}\right) = 16.99°.$$

Sketch 7.2 Wing planform with undeployed slat

The derived sweep angles $\Lambda_0 = 27.47°$ and $\Lambda_1 = 16.99°$, the parameter $A\tan\Lambda_0 = 4.16$, the Mach number and the Reynolds number all lie within the ranges shown in Table 5.2.

Determine $\Delta C_{ml w\alpha 0}$

In addition to the incremental coefficients

$$\Delta C_{ml\alpha 0} = -0.0894$$

and $$\Delta C'_{L0l} = -0.100$$

for the aerofoil section from Example 7.1, various factors are needed to determine $\Delta C_{mlw\alpha 0}$ from Equation (3.18).

The device type correlation factors K_l and $K_{l\Lambda}$ are given in Table 3.2 as

$$\begin{aligned} K_l &= 1.1 \cos\delta_l^\circ \cos\Lambda_0 \\ &= 1.1 \times \cos 35^\circ \times \cos 27.47^\circ \\ &= 0.799 \end{aligned}$$

and $$K_{l\Lambda} = 1.0.$$

From Figure 2 for $\lambda = 0.4$ and $\eta_i = 0.3$,

$$K_i = 0.48$$

and for $\eta_o = 1.0$,

$$K_o = 1.0.$$

From Figure 3d for $\lambda = 0.4$, $\eta_i = 0.3$ and $c'/c = 1.118$, using linear interpolation in c'/c,

$$K_{\Lambda i} = 0.0555$$

and for $\eta_o = 1.0$,

$$K_{\Lambda o} = 0.$$

Therefore, from Equation (3.18)

$$\begin{aligned} \Delta C_{mlw\alpha 0} &= K_l(K_o - K_i)\Delta C_{ml\alpha 0} + K_{l\Lambda}(K_{\Lambda o} - K_{\Lambda i})(A/2)\Delta C'_{L0l}\,(c'/c)\tan\Lambda_{1/4} \\ &= [0.799 \times (1.0 - 0.48) \times (-0.0894)] + [1.0 \times (0 - 0.0555) \times 8/2 \times (-0.100) \times 1.118 \times \tan 25^\circ] \\ &= -0.0371 + 0.0116 \\ &= \mathbf{-0.0255}. \end{aligned}$$

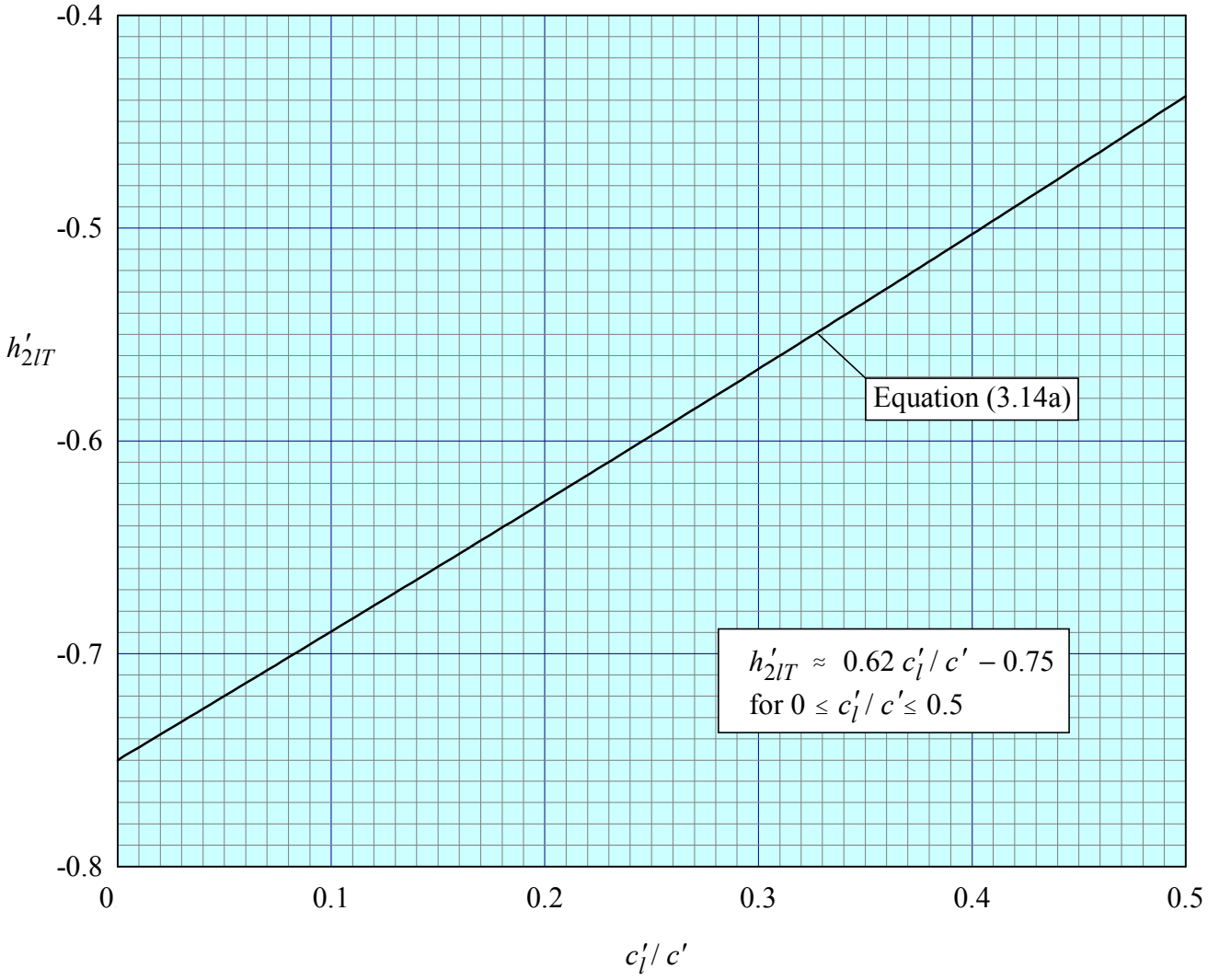

FIGURE 1 THEORETICAL CENTRE OF INCREMENTAL LIFT ON AEROFOIL DUE TO LEADING-EDGE DEVICE DEPLOYMENT

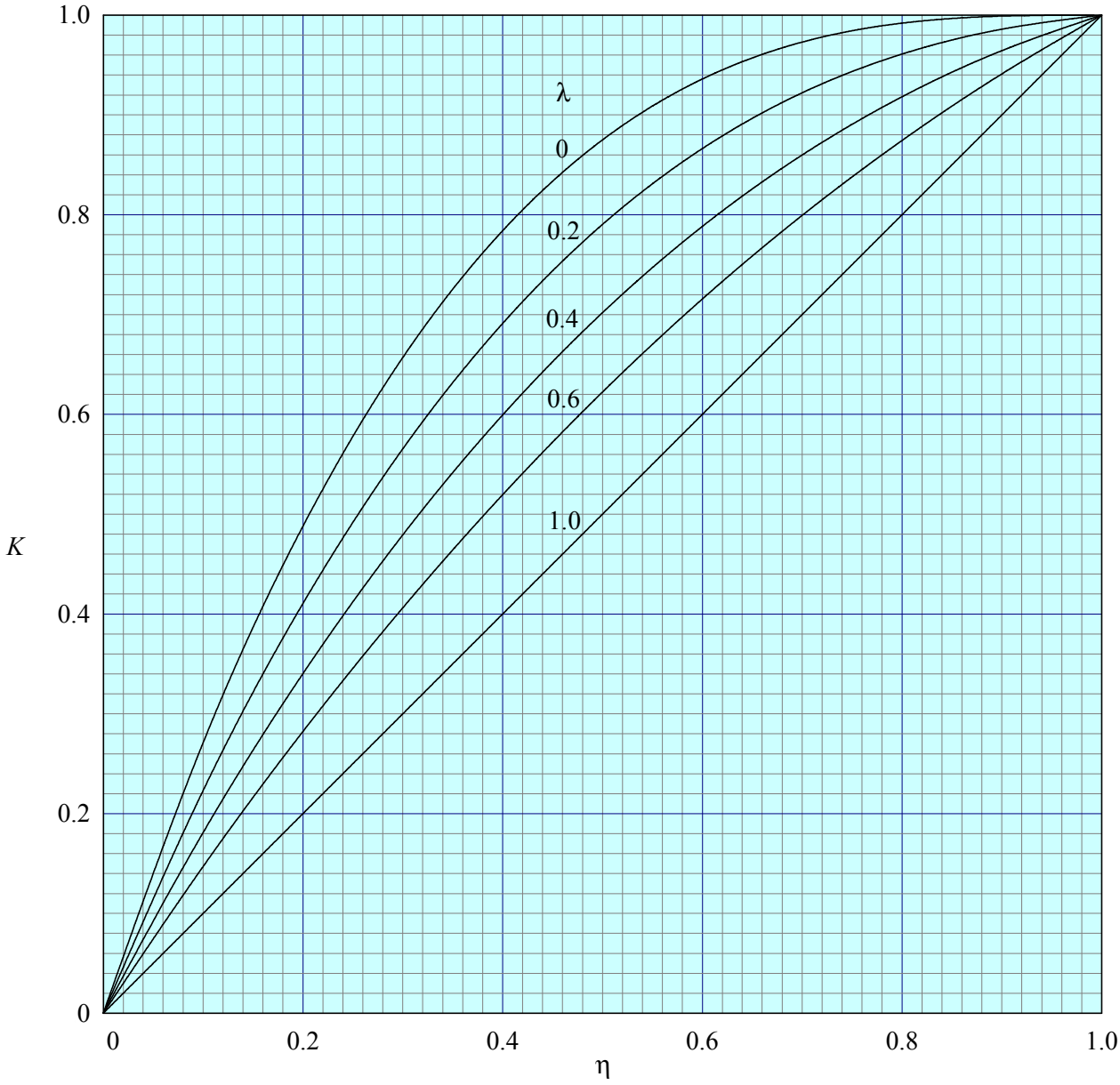

FIGURE 2 PART-SPAN FACTOR *K* FOR LEADING-EDGE DEVICES

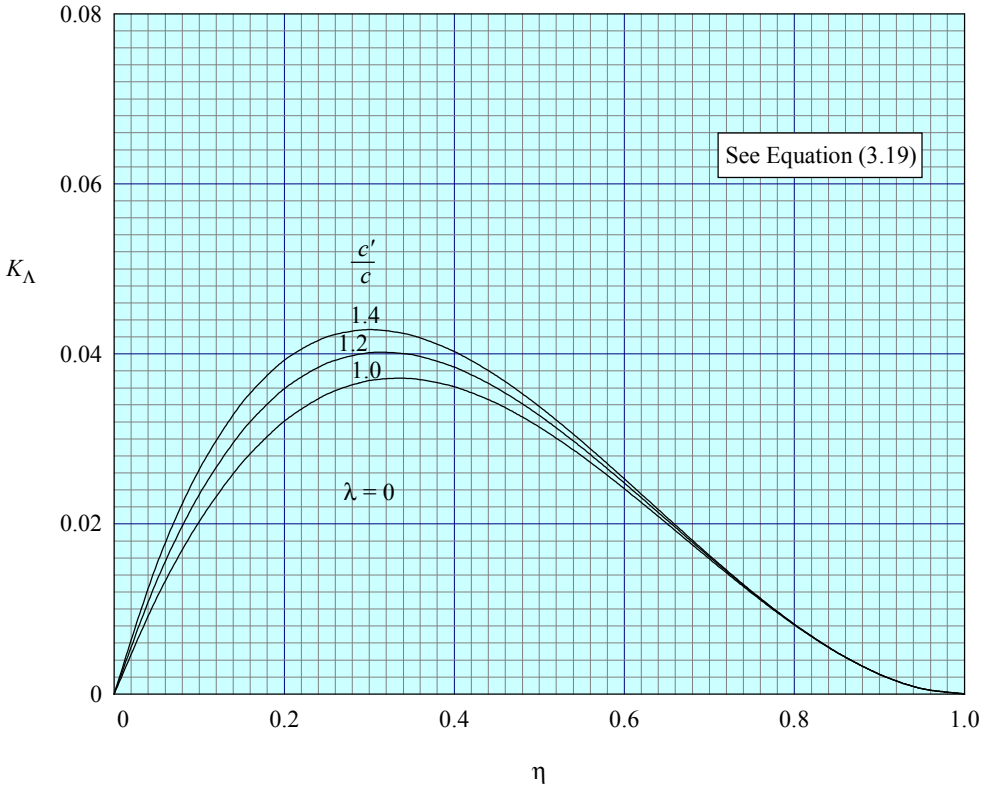

FIGURE 3a PART-SPAN FACTOR K_Λ FOR LEADING-EDGE DEVICES

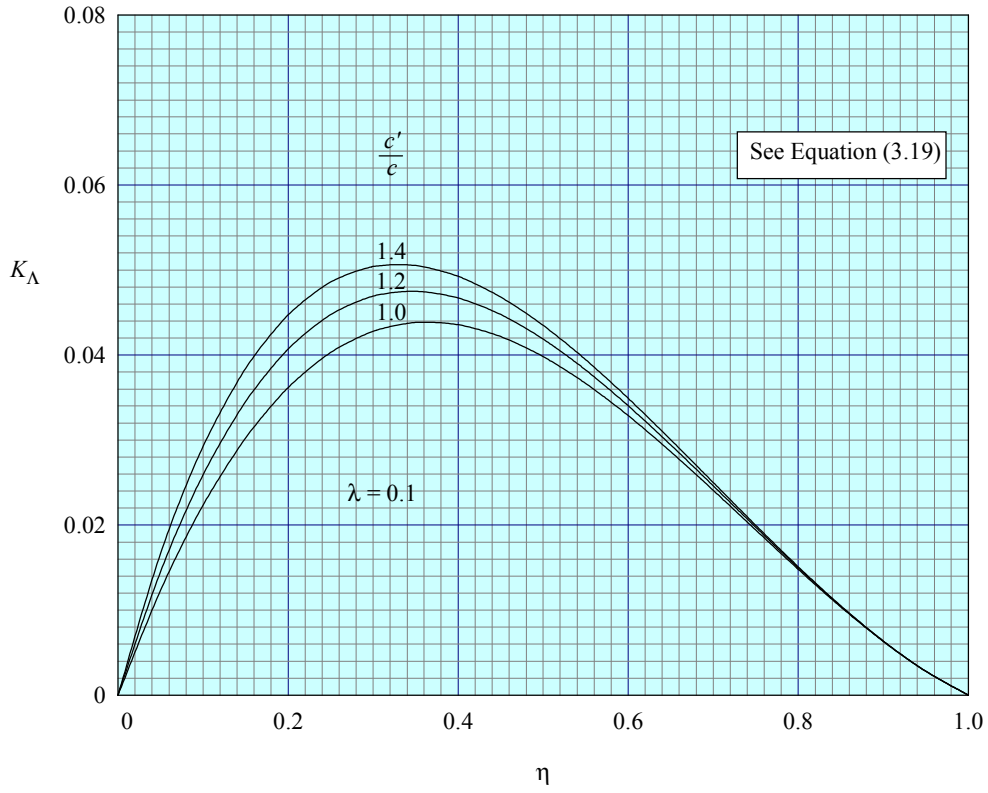

FIGURE 3b PART-SPAN FACTOR K_Λ FOR LEADING-EDGE DEVICES

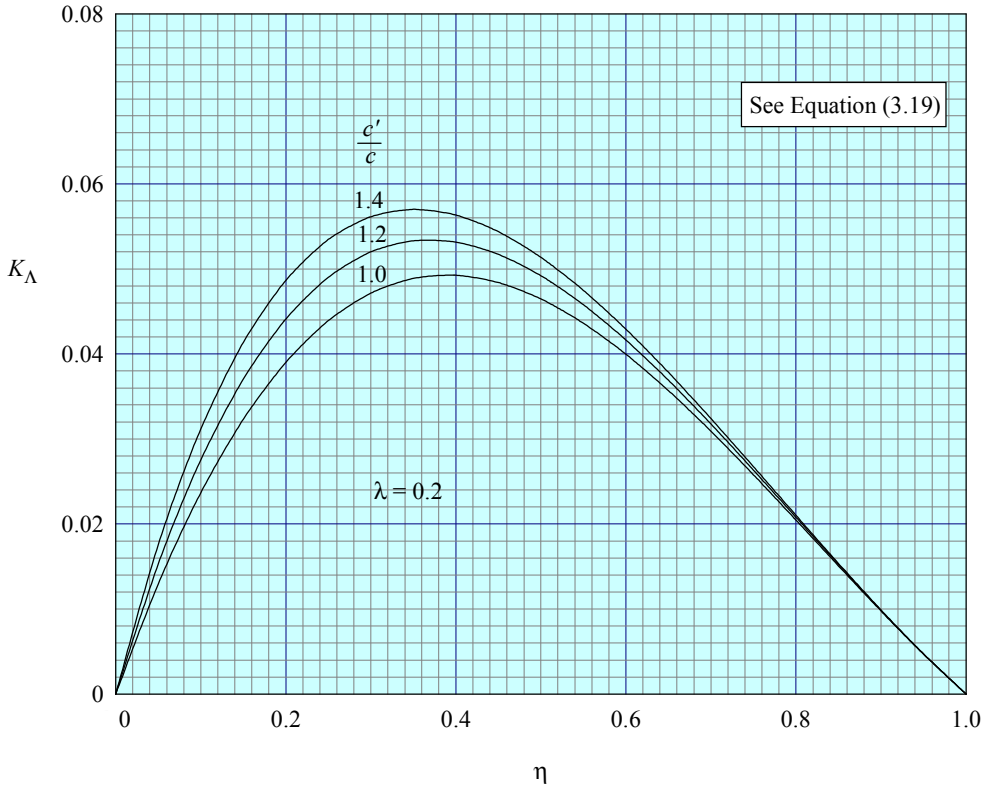

FIGURE 3c PART-SPAN FACTOR K_Λ FOR LEADING-EDGE DEVICES

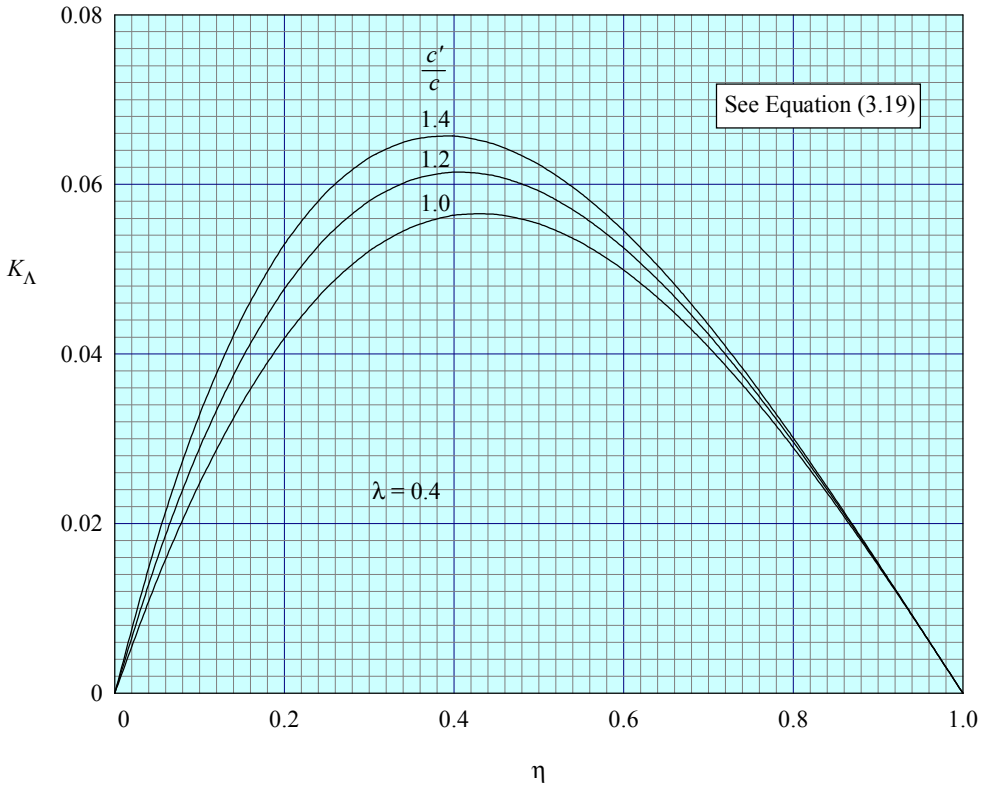

FIGURE 3d PART-SPAN FACTOR K_Λ FOR LEADING-EDGE DEVICES

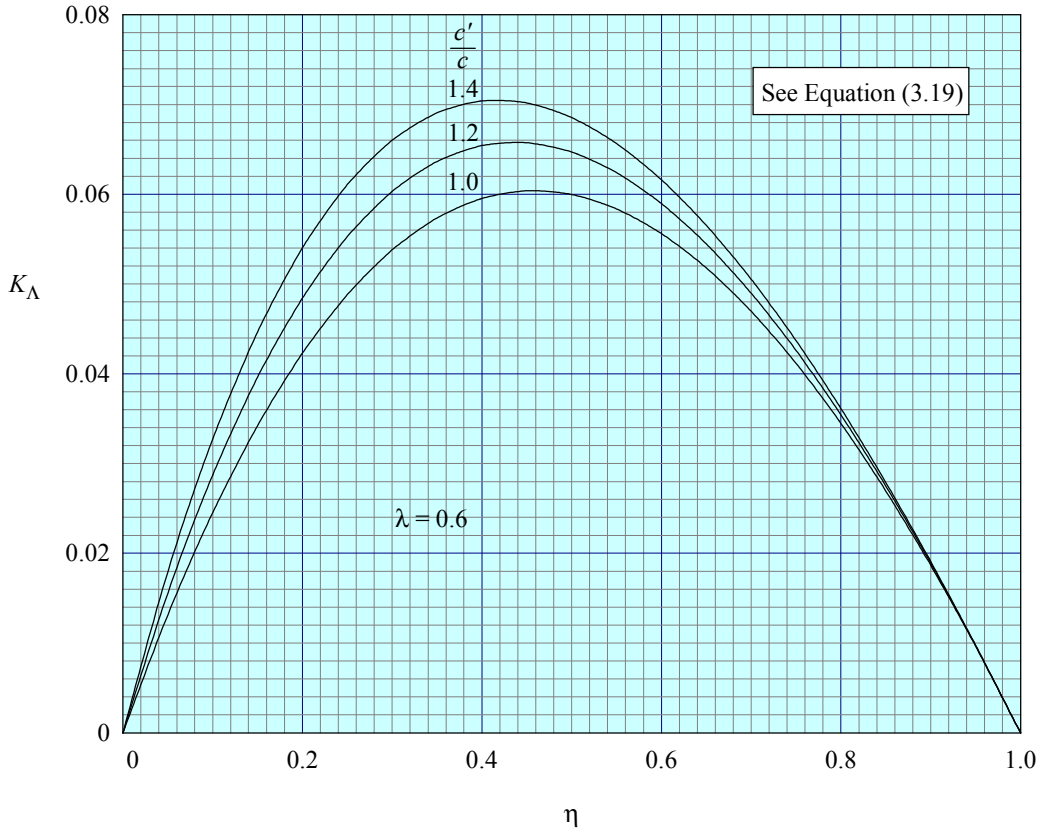

FIGURE 3e PART-SPAN FACTOR K_Λ FOR LEADING-EDGE DEVICES

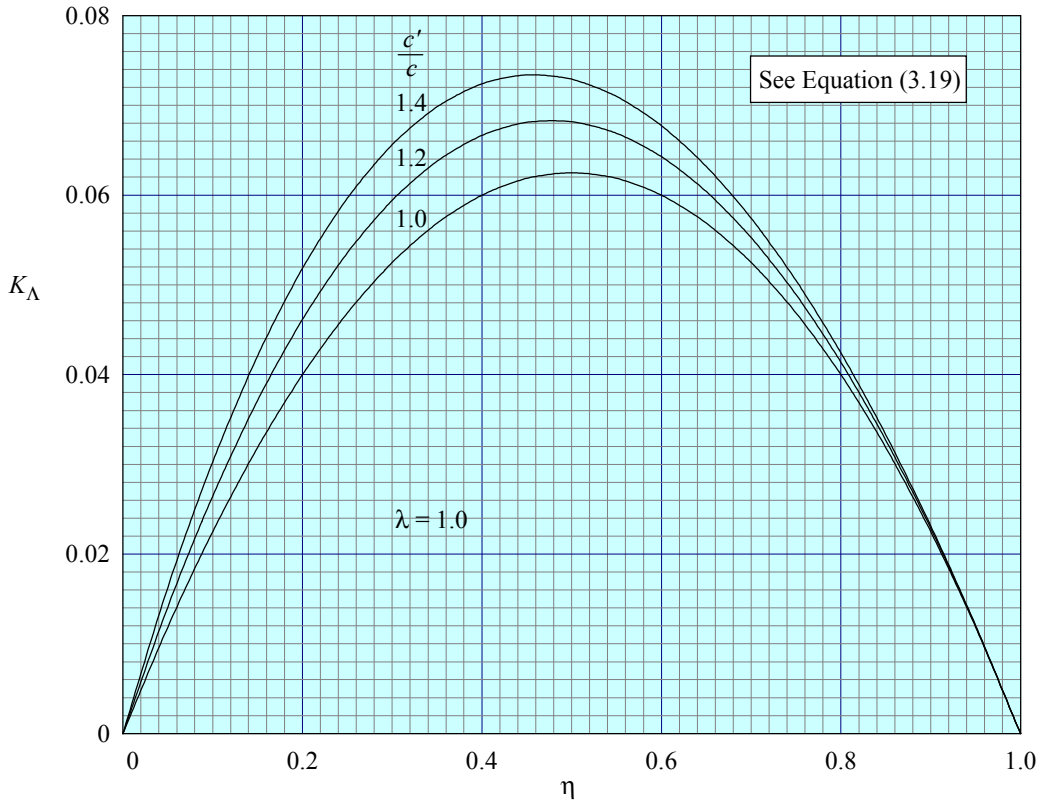

FIGURE 3f PART-SPAN FACTOR K_Λ FOR LEADING-EDGE DEVICES

KEEPING UP TO DATE

Whenever Items are revised, subscribers to the service automatically receive the material required to update the appropriate Volumes. If you are in any doubt whether your ESDU holding is up to date, please contact us.

Please address all technical engineering enquiries and suggestions to:

ESDU International plc	Tel:	020 7490 5151 (from the UK) +44 20 7490 5151 (from outside the UK)
	Fax:	020 7490 2701 (from the UK) +44 20 7490 2701 (from outside the UK)
	e-Mail:	esdu@esdu.com
	Website:	www.esdu.com

For users in the USA, please address all Customer Service and Support enquiries and suggestions to:

IHS Engineering Products and Global Engineering Documents	Tel: Fax: Website:	1 800 525 7052 (toll free number) 1 303 397 2599 www.ihs.com www.global.ihs.com

00029

Aerofoil and wing pitching moment coefficient at zero angle of attack due to deployment of leading-edge high-lift devices at low speeds
ESDU 00029

ISBN 1 86246 132 5, ISSN 0141-397X

Available as part of the ESDU Series on Aerodynamics. For information on all ESDU validated engineering data contact ESDU International plc, 27 Corsham Street, London N1 6UA.

ESDU 00029 predicts for aerofoils the centre of lift position based on thin-aerofoil theory with empirical correction. This is combined with the predicted increment in aerofoil lift coefficient from ESDU 94027 to estimate the pitching moment coefficient increment. For wings with full-span leading-edge devices, factors dependent on planform geometry are applied to the pitching moment coefficient increment on an aerofoil section that is representative of the wing in order to allow for three-dimensional effects. For wings with part-span devices, additional factors are introduced that are dependent on the wing taper ratio and on the spanwise extent of the devices, and the effect of wing aspect ratio and sweep is also accounted for in the procedure. The method covers plain leading-edge flaps, drooped leading edges, slats, sealed slats, and vented and unvented Krüger flaps. It applies in free air and at Mach numbers below 0.2. Sketches illustrate the accuracy of prediction and tables give the ranges of parameters covered in the construction of the method. For aerofoils, 80 per cent of the data for the increment in pitching moment coefficient are predicted to within 0.005. For wings, 95 per cent of the data for the increment in pitching moment coefficient are predicted to within 0.010. A worked example illustrates the use of the method.

© ESDU International plc, 2000

All rights are reserved. No part of any Data Item may be reprinted, reproduced, or transmitted in any form or by any means, optical, electronic or mechanical including photocopying, recording or by any information storage and retrieval system without permission from ESDU International plc in writing. Save for such permission all copyright and other intellectual property rights belong to ESDU International plc.

ESDU™
Engineering Sciences Data Unit
An IHS GROUP Company